CAMS Solar radiation products Regular Validation Report, Issue #31, June-Aug. 2020

Mireille Lefèvre

ECMWF COPERNICUS REPORT
Copernicus Atmosphere Monitoring Service

D72.1.3.1
Regular Validation Report
Issue #31
J-J-A 2020

CAMS-72
Solar radiation products

Issued by: Armines / M. Lefèvre

Date: 26/03/2021

Ref: CAMS72_2018SC2_D72.1.3.1-2021Q1_RAD_validation_report_JJA2020_v1

Contributors

ARMINES
Mireille Lefèvre

Table of Contents

Executive summary 7

1 Introduction 9

2 Stations 10

2.1 Maps 10
2.2 List of the stations retained for this quarter 12
2.3 Quality check 14

3 Overview of the results 17

3.1 Bias and standard deviation of errors 17
3.2 Ability to reproduce the intra-day variability 20
3.3 Ability to reproduce the frequency distributions of measurements 23
3.4 Ability to reproduce the monthly means and standard deviation for the period 29
3.5 Multi-annual statistical indicators 31
3.5.1 Global irradiance 32
3.5.2 Diffuse irradiance 34
3.5.3 Direct normal irradiance 36
3.6 Recommendations 37

4 Sources of data 38

4.1 Sources of data 38
4.2 Short description of the stations selected for the validation 39
4.3 Evolution of the list of stations 42
4.4 Stations under evaluation 42
4.4.1 Cairo (Egypt) 42
4.4.2 Zagora (Morocco) 45
4.4.3 Erfoud (Morocco) 46
4.4.4 Oujda (Morocco) 47

5 Acknowledgements 48

6 Reference documents 49

Annex A. Procedure for validation 51

A.1 Controlling the quality of the observations and taking care of the time system 51
A.2 Taking care of missing observations within an hour or one day 51
A.3 Pairing observations and estimates 52

A.4 Overview of the procedure for validation **52**
A.5 Computation of deviations and statistical quantities **52**
A.6 Typical uncertainty of measurements **55**
A.7 Definitions of a few quantities in solar radiation **56**

Annex B. Station validation reports for this quarter **58**

Executive summary

The CRS is continuously monitored against ground-based irradiance observations. This includes stations in various geographical locations and climates (see maps in Fig. 2.1 and Fig. 2.2 and description in section 4.2). Several stations being affected by large satellite viewing angles are included by intention to provide quantitative insight where the CRS may become unreliable for some applications (Tab. 2.1). From this #31 issue onwards, a new table of the ground datasets performance is presented with the amount of data rejected / retained for each station by the quality check (Tab. 2.2).

From the last #30 issue onwards, the protocol of validation (see Annex A.5) has been changed regarding the threshold applied for the usable measurements. For the consistency, the same new protocol has been applied to every JJA quarter in the multi-annual plots.

For JJA 2020, the correlation is very good for global (*G*, Fig. 3.4), good for beam irradiances *(B*, Fig. 3.6) except stations Oujda, Cairo (stations with frequent problems of maintenance) and Izaña, and rather good for diffuse (*D*, Fig. 3.5) except EnerMENA stations and Izaña. It should be noted that all stations with low satellite viewing have good performance for *G*, *D* and *B*. Regarding the clearness indices, the beam KT_B are at the same level as for *B* for all stations. The global KT_G and diffuse KT_D correlations are lower than those for *G* and *D* for all stations. They give good performances for global KT_G, but poor performance for diffuse KT_D.

In absolute value the bias for the global irradiance is null or low for 7 stations and noticeable or large for 23 stations out of 30 (Tab. 3.1). In term of relative value, the bias is under 7 % for most stations. The bias is positive (overestimation) for all stations with low KT_G (frequent cloudy skies) and more often negative (underestimation) for the stations with frequent clear skies (Fig. 3.1). It was already observed for the previous MAM 2020 period. Actually, at all stations the CRS clearness index KT_G in range [0.5, 0.7] is over-represented (Fig. 3.8). For stations with frequent cloudy skies it is done at the expense of the lower $KT_G < 0.2$ and higher $KT_G > 0.7$, i.e., *G* is roughly overestimated for the cloudy skies. For the stations with frequent clear skies, it is done at the expense of higher $KT_G > 0.7$, i.e., *G* is underestimated for the clear skies.
The station Izaña, at high altitude, presents the best frequency distribution of KT_G and good performance for the bias and the RSME although correlation is not good.
The multi-annual indicators highlight a small degradation of the performance for this JJA quarter in 2020 (CY46R1) compared to year 2018 (CY45R1), but a much better performance compared to 2016-2017 years (Fig. 3.16b).

The bias for the diffuse irradiance (Fig. 3.2) is null or low for 7 stations and noticeable or large for 10 stations out of 17. The frequency distributions (Fig. 3.10) of the $KT_D < 0.1$ are clearly under-represented for the benefit of KT_D in the range [0.1, 0.3], i.e., low *D* are always overestimated.

Izaña exhibits a much more correct frequency distribution, along with an over-representation of the low $KT_D < 0.2$ contrary to other stations. The multi-annual indicators (Fig. 3.17b) show worse results for EnerMENA stations although no significant evolution over the years can be pointed out because of lack of data for year 2018-2019. Another issue is the lack of maintenance of some EnerMENA stations during June 2020.

Such as *G*, the bias for the direct normal irradiances (Fig. 3.3) is more often positive (overestimation) for the stations with low KT_B (frequent cloudy skies) and more often negative (underestimation) for the stations with frequent clear skies. That is also illustrated in the frequency distributions of *B* (Fig. 3.11) and KT_B (Fig. 3.12). The lowest $KT_B < 0.1$ are under-represented at stations with a positive bias, while the medium KT_B [0.2, 0.5] are over-represented at the expense of higher KT_B at stations with negative bias. Such as D, the multi-annual indicators evolution (Fig. 3.18b) is difficult to interpret because of lack of data for the JJA periods in the previous years. Kauno and Silutes have beneficiated of a renovation at the beginning of 2020, and exhibits from then much better results.

The monthly means of the estimated *G* (Fig. 3.13) are identical or close to those of the measurements at all stations. In desertic climates *G* is slightly underestimated while it is slightly overestimated in other regions. As for *D* (Fig. 3.14) and *B* (Fig. 3.15) the discrepancies rely overall on Izaña and the desertic stations, with lower dynamics for the estimated values compared to measurements.
The monthly standard deviations that highlight the dynamics of the dataset are generally low at most stations. This underestimation is null or slight for *G*.

As a whole, the frequency distributions of measurements of hourly means, expressed as binned histograms, are not well represented by CRS, although correlations are quite good. It should be noted that the BSRN station Izaña, at a high altitude, presents the inverse pattern. For the 3 components, a loss of dynamics is generally observed for the estimated values compared to measurements. For the stations with frequent cloudy skies, the frequency of the lowest irradiances is too low (irradiances are overestimated, or clouds not well detected). For the stations with frequent clear skies, the frequency of the highest irradiances is too low (irradiances are underestimated, or clouds detected when there are absent). That is in accordance with the frequent observations of low monthly standard deviations mentioned above.

Stations with low satellite viewing angle give good results, while some enerMENA stations often give weak results. This could be due to the frequent deposition of particulate matter in these desertic regions together with frequent problems of maintenance (see Table 2.1 and section 4.4) especially during this covid-19 period.
Surprisingly, Izaña, at a high altitude (2373 m) presents the best frequency distributions for G, *D* and *B*, with rather good performance with *G* indicators, although indicators are quite bad for *D* and weak for *B*.

1 Introduction

The CAMS Radiation Service, abbreviated as CRS, delivers estimates of the solar radiation arriving at ground level on a horizontal surface. Outcomes of the CRS have to be validated on a periodic basis. Following practices in CAMS, this validation is performed every quarter. Following current practices, the CRS irradiances are tested against qualified ground measurements measured at several ground-based stations serving as reference. These ground measurements are coincident in time with the CRS estimates.
This report is issue #31 of a regular report. It deals with hourly means of global, diffuse, and direct irradiances for the period June-July-August 2020, abbreviated as JJA 2020.

On 2017-10-11, version 3 of the CRS was introduced. By construction, the CRS performs the calculation of the radiation on-the-fly at the request of any user. It processes on-the-fly the necessary information that is stored in CAMS and does not create a proper database of the results. Hence, the new version 3 applies from now on back to 2004-02-01. This validation report is performed with version 3 of the CRS. Issues #17 and #19 of this report comprise comparisons between v2 and v3.

In #24 of this report a multi-annual assessment of the respective season was introduced. This has made the quarterly validation reports very large. Therefore, from issue #25 onwards detailed results are partly provided in a zip archive supplement as individual files in a well-organized folder structure.

The results discussed in this report may also be retrieved for several of the selected stations and others by running the service “Irradiation Validation Report” on the SoDa website: http://www.soda-pro.com/fr/web-services/validation/irradiation-validation-report . This service “Irradiation Validation Report” performs a comparison of the hourly or daily solar irradiation at surface estimated by the CRS against several qualified ground measurements obtained from various sources. It returns a HTML page that contains statistics of comparisons and graphs. Similar calculations can be done for the estimates of solar radiation from the HelioClim-3 databases, allowing comparisons with the CRS.

2 Stations

The source of ground-based measurements is given in section 4, along with a description of each station and the products provided: *G*, *B*, *D* are global, beam and diffuse irradiances respectively, and KT_G, KT_B, KT_D are global, beam and diffuse clearness indices, respectively. These parameters are defined in Annex A.7.

2.1 Maps

Figure 2.1 (Europe) and Figure 2.2 (other regions) show the location of the stations as reported in Table 4.2. Symbols code the initial summarization of the data as reported in Table 4.1: circle for 1 min, and downward triangle for 1 h. Colors code the type of data at each site: red for (*G, B, D*), yellow for (*G, B*), magenta for (*G, D*) and cyan for *G*.

In the last #27 report, some stations have been removed from the set of usual stations, and some others have been added (see Fig. 2.3 in #27). Stations too close to the sea like Hoorn (see 4.1.1 in #27 for the report of the problem) and Vlissingen in the Netherlands have been removed and replaced by Leeuwarden and Maastricht (Fig. 2.3). Stations have been closed by the providers like Carpentras and Dobele in December 2018, Rucava in September 2018, or are not updated regularly like PSA (year 2017 was provisioned in December 2018, years 2018 and 2019 was provisioned in April 2020). New stations offset these removals like CENER in Spain, or Aluksne and Kolka, two new stations provided monthly by the Latvian network instead of Dobele and Rucava. Since November 2019, the enerMENA network provides a new station Fki-Ben-Salah in Morocco. In this #31 report, the KNMI station of Cabauw has been replaced with the same station provided by the BSRN network that offers the 3 components *G*, *D* and *B* at 1 min of resolution. The BSRN station of Izaña has been added for evaluation at a high altitude.

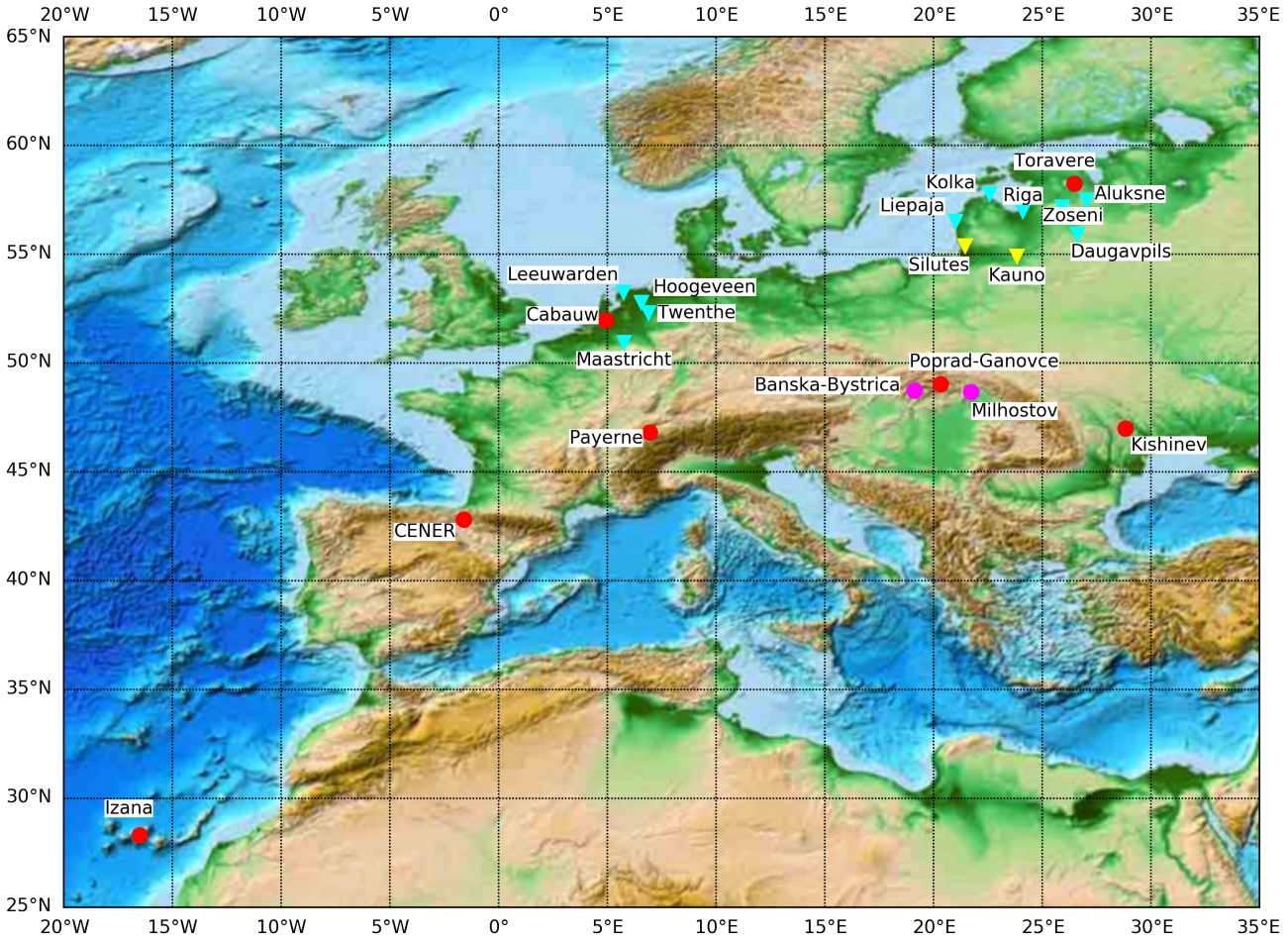

Figure 2.1. Map showing the 21 stations in Europe. Symbols code the initial summarization: circle for 1 min, and downward triangle for 1 h. Colors code the type of data at each site: red for (*G, B, D*), yellow for (*G, B*), magenta for (*G, D*) and cyan for *G*.

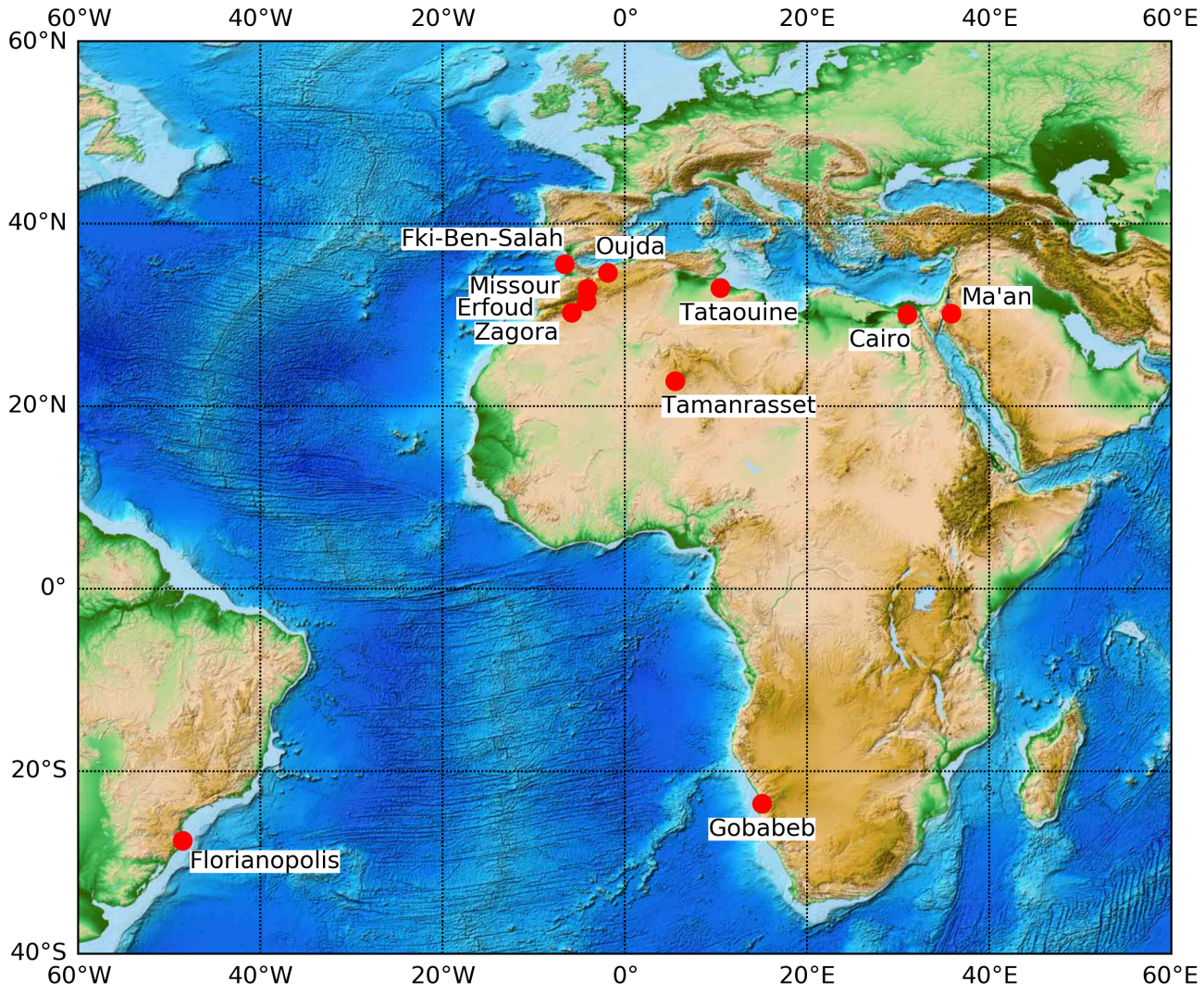

Figure 2.2. Map showing the 11 stations outside Europe. Symbols code the initial summarization: circle for 1 min, and downward triangle for 1 h. Colors code the type of data at each site: red for (*G, B, D*), yellow for (*G, B*), magenta for (*G, D*) and cyan for *G*.

2.2 List of the stations retained for this quarter

Depending on the provision of fresh data, possible problems affecting measuring instruments, possible rejection of some data by the quality control, and other causes, it is not always possible to use the same set of stations to perform the quarterly validation. Table 2.1 lists the 30 stations that have been retained for this quarter, along with the 2 stations usually retained but having no available data for this quarter.

Due to low satellite viewing angles, lower CRS quality is expected for stations in Lettland and Lithuania (Aluksne, Daugavpils, Kauno, Kolka, Liepaja, Riga, Silutes, Toravere) and Brazil (Florianopolis). Nevertheless, stations in Lettland and Lithuania provide some insight on the area where the CRS may become unreliable and therefore, this information is kept in this user-oriented report. The same reason motivates the new addition of Izaña at a high altitude.

From this #31 report onwards, a summary of the quality check operated on each station is given in Table 2.2 (section 2.3).

Table 2.1. List of stations retained or excluded for this regular validation report.

Station	Variables	Issues for the period
Aluksne	*G - -*	Reduced service accuracy expected due to low satellite viewing angle.
Banska-Bystrica	*G D -*	
Cabauw	*G D B*	**From issue #31 onwards, the KNMI dataset with 1 h resolution and only G component is replaced with the BSRN dataset offering 1 min resolution and the 3 components**.
Cairo	*G D B*	**Doubtful maintenance of the sensor during this COVID-19 period. Tracking failure in June.**
CENER	*G D B*	
Daugavpils	*G - -*	Reduced service accuracy expected due to low satellite viewing angle.
Erfoud	*G D B*	
Florianopolis	*G D B*	Reduced service accuracy expected due to low satellite viewing angle.
Fki-Ben-Salah	*- D B*	***G* not available due to a broken sensor. Pyrheliometer sometimes misaligned due to erroneous mounting. Cleaning button broken.**
Gobabeb	*G D B*	
Hoogeveen	*G - -*	
Izaña	*G D B*	New station to be evaluated for regular validation. Reduced service accuracy expected due to altitude 2372 m.
Kauno	*G - B*	Renovation of the equipment at the beginning of 2020. The station is under long-term evaluation (see section 4) as results are often bad. Reduced service accuracy expected due to low satellite viewing angle.
Kishinev	*G D B*	
Kolka	*G - -*	Reduced service accuracy expected due to low satellite viewing angle.
Leeuwarden	*G - -*	
Liepaja	*G - -*	Reduced service accuracy expected due to low satellite viewing angle.
Ma'an	*G D B*	**No cleaning of the sensor in June due to COVID-19 period.**
Maastricht	G - -	
Milhostov	*G D -*	
Missour	*G D B*	Many short (June-July) or long (August) data gaps due to power failures of the logger.

Station	Variables	Issues for the period
Oujda	*G D B*	**Tracker failure between 8 and 16 of June 2020.**
Payerne	*G D B*	No data available from February 2020 onwards.
Poprad-Ganovce	*G D B*	
Riga	*G - -*	Reduced service accuracy expected due to low satellite viewing angle.
Silutes	*G - B*	Renovation of the equipment at the beginning of 2020. A long-term monitoring of this station is ongoing (see section 4). Reduced service accuracy expected due to low satellite viewing angle.
Tamanrasset	*G D B*	Only *G* is available. *D* and *B* unavailable from March 2018 onwards.
Tataouine	*G D B*	**Medium quality in June 2020.**
Toravere	*G D B*	**No data available from June 2020 onwards.** Reduced service accuracy expected due to low satellite viewing angle.
Twenthe	*G - -*	
Zagora	*G D B*	
Zoseni	*G - -*	Reduced service accuracy expected due to low satellite viewing angle.

2.3 Quality check

Table 2.2 summarizes for each station:

- The number of usable values in the ground dataset expressed as a percentage of the number of daylight instants in the JJA period, i.e., the number of instants corresponding to the source resolution (1 h or 1 min) for a solar zenith angle SZA <= 89°.

- The number of values rejected by the quality check (QC) expressed as a percentage of the usable values in the ground dataset.

- The number of retained values in the ground dataset after the quality check, expressed as a percentage of the number of daylight instants in the JJA2020 period. That represents the dimension of the ground dataset before the summarization to hourly resolution and the application of the SZA threshold.

Table 2.2. Quantities of ground measurements rejected or retained for each station in the JJA 2020 period.

Station	Variable	Daylight instants during the period	Observation >=0 during daylight before QC		QC Test	Data rejected by the QC during daylight		Observation >=0 during daylight after QC and before SZA threshold	
		N	N	%		N	%	N	%
Aluksne	*G*	1504	1504	100	BSRN-1C	0	0,000	1504	100
Banska-Bystrica	*G*	82291	82232	100	BSRN-2C	36	0,044	82196	100
	D	82291	82228	100		32	0,039	82196	100
Cabauw	*G*	84450	84227	100	BSRN-3C	1049	1,245	83178	99
	D	84450	84258	100		1080	1,282	83178	99
	B	84450	83550	99		372	0,445	83178	99
Cairo	*G*	73896	62702	85	BSRN-3C	2463	3,928	60239	82
	D	73896	60651	82		412	0,679	60239	82
	B	73896	63129	85		2890	4,578	60239	82
CENER	*G*	79040	78083	99	BSRN-3C	4125	5,283	73958	94
	D	79040	78086	99		4128	5,286	73958	94
	B	79040	74212	94		254	0,342	73958	94
Daugavpils	*G*	1440	1419	99	BSRN-1C	0	0,000	1419	99
Erfoud	*G*	74398	74285	100	BSRN-3C	34	0,046	74251	100
	D	74398	74264	100		13	0,018	74251	100
	B	74398	74375	100		124	0,167	74251	100
Fki-ben-Salah	*D*	74781	60649	81	BSRN-1C	52	0,086	60597	81
	B	74781	61819	83		0	0,000	61819	83
Florianopolis	*G*	57605	56969	99	BSRN-3C	447	0,785	56522	98
	D	57605	56938	99		416	0,731	56522	98
	B	57605	56551	98		29	0,051	56522	98
Gobabeb	*G*	58939	58895	100	BSRN-3C	101	0,171	58794	100
	D	58939	58906	100		112	0,190	58794	100
	B	58939	58851	100		57	0,097	58794	100
Hoogeveen	*G*	1433	1433	100	BSRN-1C	0	0,000	1433	100
Izaña	*G*	73305	70811	97	BSRN-3C	116	0,164	70695	96
	D	73305	71721	98		1026	1,431	70695	96
	B	73305	71748	98		1053	1,468	70695	96
Kauno	*G*	1460	1459	100	BSRN-1C	0	0,000	1459	100
	B	1460	1459	100		39	2,673	1420	97
Kishinev	*G*	1381	1379	100	BSRN-3C	58	4,206	1321	96

Station	Variable	Daylight instants during the period	Observation >=0 during daylight before QC		QC Test	Data rejected by the QC during daylight		Observation >=0 during daylight after QC and before SZA threshold	
		N	N	%		N	%	N	%
	D	1381	1343	97		22	1,638	1321	96
	B	1381	1342	97		36	2,683	1306	95
Kolka	*G*	1510	1510	100	BSRN-1C	0	0,000	1510	100
Leeuwarden	*G*	1436	1436	100	BSRN-1C	0	0,000	1436	100
Liepaja	*G*	1470	1446	98	BSRN-1C	0	0,000	1446	98
Maan	*G*	29447	29311	100	BSRN-3C	288	0,983	29023	99
	D	29447	29121	99		98	0,337	29023	99
	B	29447	29310	100		287	0,979	29023	99
Maastricht	*G*	1392	1392	100	BSRN-1C	0	0,000	1392	100
Milhostov	*G*	82240	82183	100	BSRN-2C	24	0,029	82159	100
	D	82240	82180	100		21	0,026	82159	100
Missour	*G*	74874	43046	58	BSRN-3C	152	0,353	42894	57
	D	74874	42987	57		93	0,216	42894	57
	B	74874	43264	58		370	0,855	42894	57
Oujda	*G*	75542	75025	99	BSRN-3C	11461	15,276	63564	84
	D	75542	65126	86		1562	2,398	63564	84
	B	75542	75496	100		11932	15,805	63564	84
Poprad-Ganovce	*G*	82473	82412	100	BSRN-3C	3518	4,269	78894	96
	D	82473	82393	100		3499	4,247	78894	96
	B	82473	79267	96		373	0,471	78894	96
Riga	*G*	1490	1490	100	BSRN-1C	0	0,000	1490	100
Silutes	*G*	1463	1463	100	BSRN-1C	0	0,000	1463	100
	B	1463	1463	100		18	1,230	1445	99
Tamanrasset	*G*	71590	68441	96	BSRN-1C	1	0,001	68440	96
Tataouine	*G*	74927	60760	81	BSRN-3C	5	0,008	60755	81
	D	74927	60760	81		5	0,008	60755	81
	B	74927	60761	81		6	0,010	60755	81
Twenthe	*G*	1425	1425	100	BSRN-1C	1	0,070	1424	100
Zagora	*G*	73970	73095	99	BSRN-3C	6	0,008	73089	99
	D	73970	73094	99		5	0,007	73089	99
	B	73970	73171	99		82	0,112	73089	99
Zoseni	*G*	1495	1495	100	BSRN-1C	0	0,000	1495	100

3 Overview of the results

Following the ISO standard (1995), the deviations are computed by subtracting observations for each instant from the product estimations (CRS - measurements), and are summarized by usual statistical quantities such as the bias or the root mean square error. The validation procedure is described in Annex A. Detailed results for the report's season are given for each station in Annexes B.

3.1 Bias and standard deviation of errors

Detailed tables for the JJA 2020 quarter summarize the performance of the CRS for hourly means of global irradiance (in W m^{-2}, Tab. 3.1), corresponding clearness index (Tab. 3.2), and the performances relative to the mean of measurements (in percent, Tab. 3.3). Similar detailed tables are given for the *D* component (Tab. 3.4 to 3.6) and the *B* component (Tab. 3.7 to 3.9). They are available as an excel file in a folder of the supplemental zip archive:

CAMS72_2018SC2_D72.1.3.1-2021Q1_section3_statistical_metrics/
CAMS72_2018SC2_D72.1.3.1-2021Q1_section3_statistical_metrics_JJA2020.xlsx

Table 3.1 summarizes the performance of CRS for the hourly mean of irradiances. The following empirical rules adopted for the bias are derived from the uncertainty (20 W m^{-2}) of the measurements of hourly irradiation of good quality from the recommendations of the WMO (see Annex A, Table A.1).

Table 3.1. Number of stations in each category of bias (in W m^{-2})

Rules for the bias (in W m^{-2})		G	D
Null bias	Absolute value of the bias ≤ 5	2	4
Low bias	5 < absolute value of the bias ≤ 10	5	3
Noticeable bias	10 < absolute value of the bias ≤ 20	12	4
Large bias	20 < absolute value of the bias ≤ 60	10	6
Very large bias	Absolute value of the bias > 60	1	0
Number of stations		30	17

Relative biases and RMSE are given in Figures 3.1, 3.2 and 3.3 for respectively *G*, *D* and *B*.

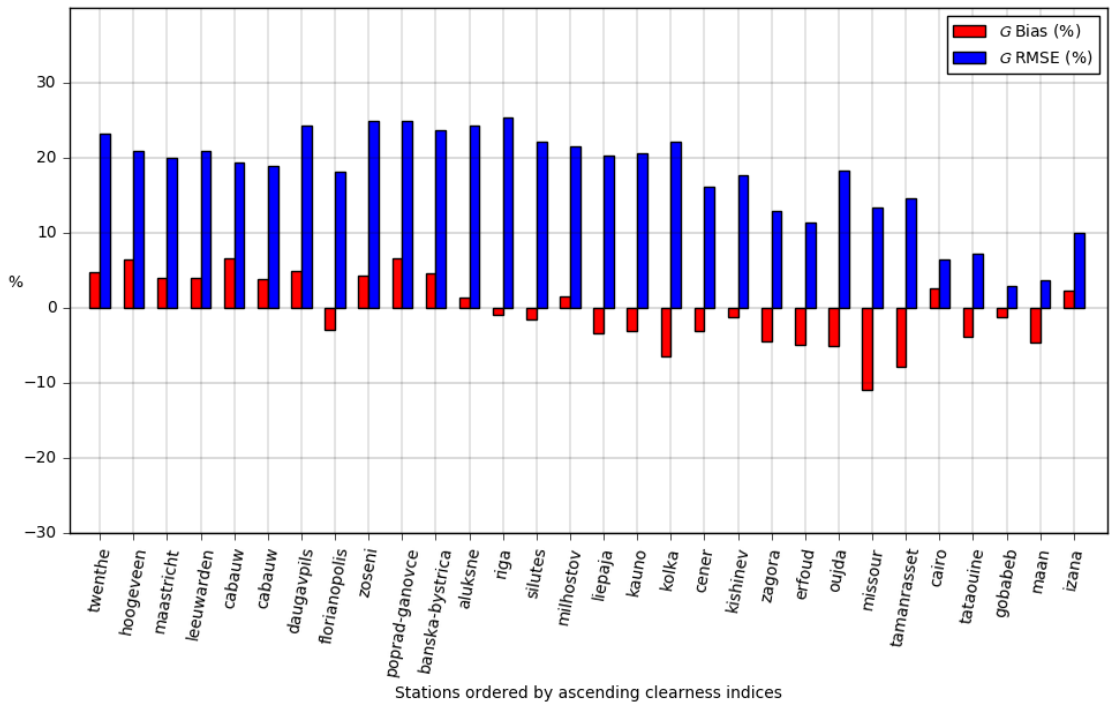

Figure 3.1. Relative bias and RMSE for global irradiance.

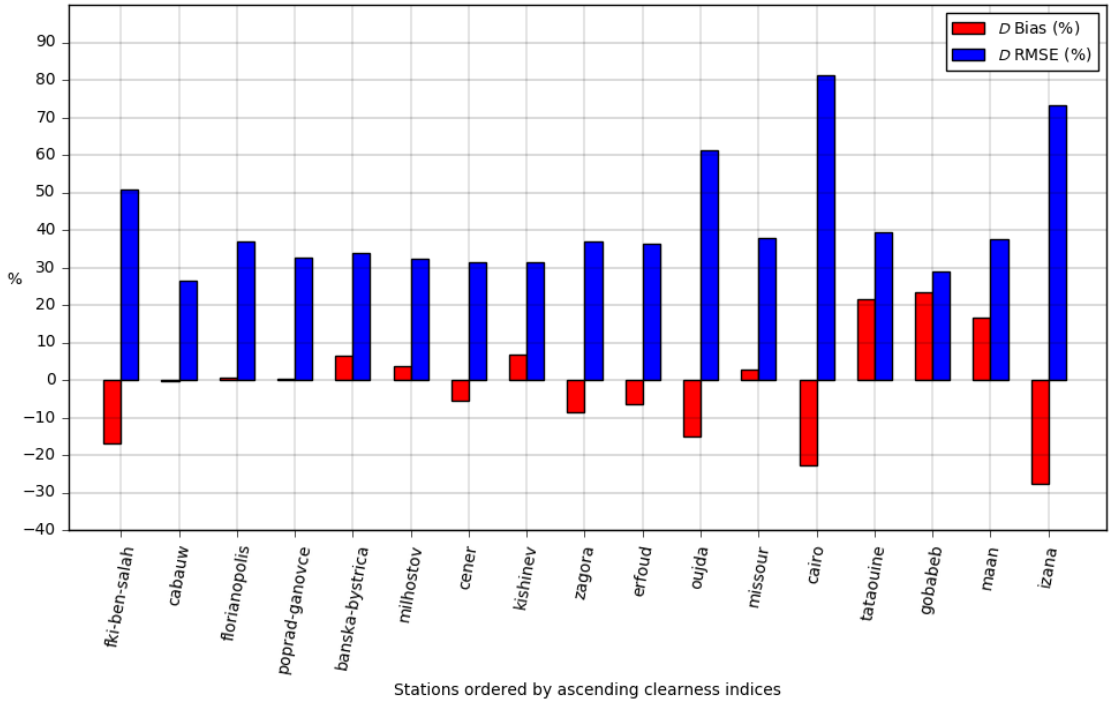

Figure 3.2. Relative bias and RMSE for diffuse irradiance.

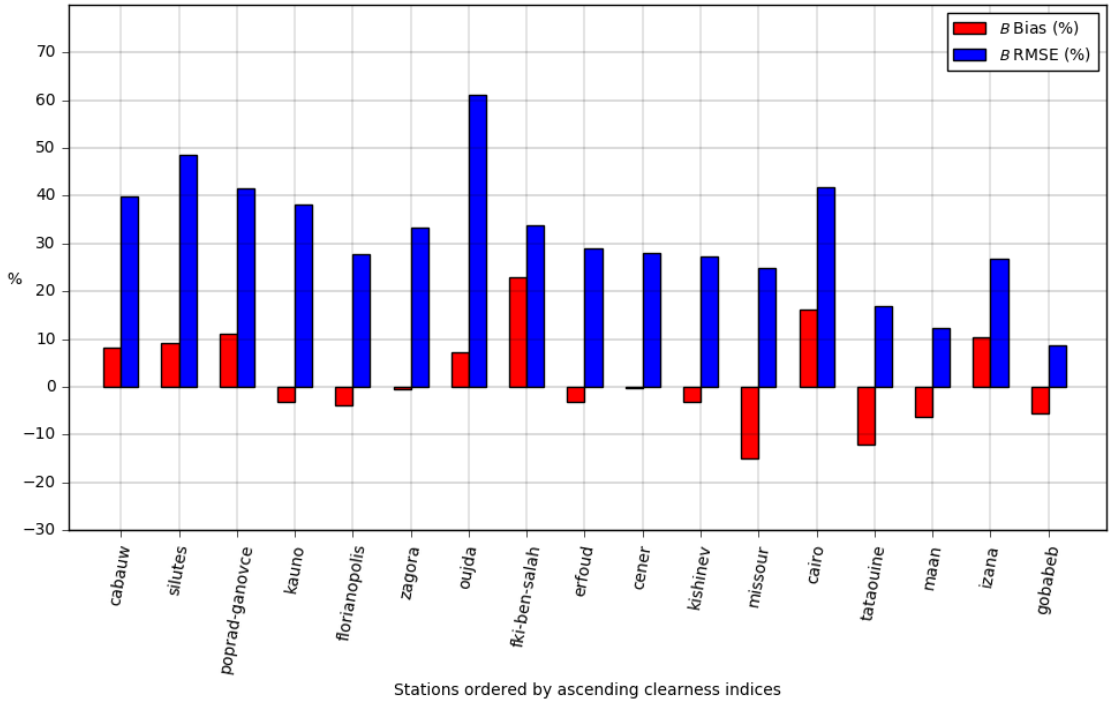

Figure 3.3. Relative bias and RMSE for direct irradiance.

3.2 Ability to reproduce the intra-day variability

The correlation coefficients of the JJA 2020 quarter are displayed for irradiances and clearness indices: G and KT_G (Fig. 3.4), D and KT_D (Fig. 3.5), B and KT_B (Fig. 3.6).

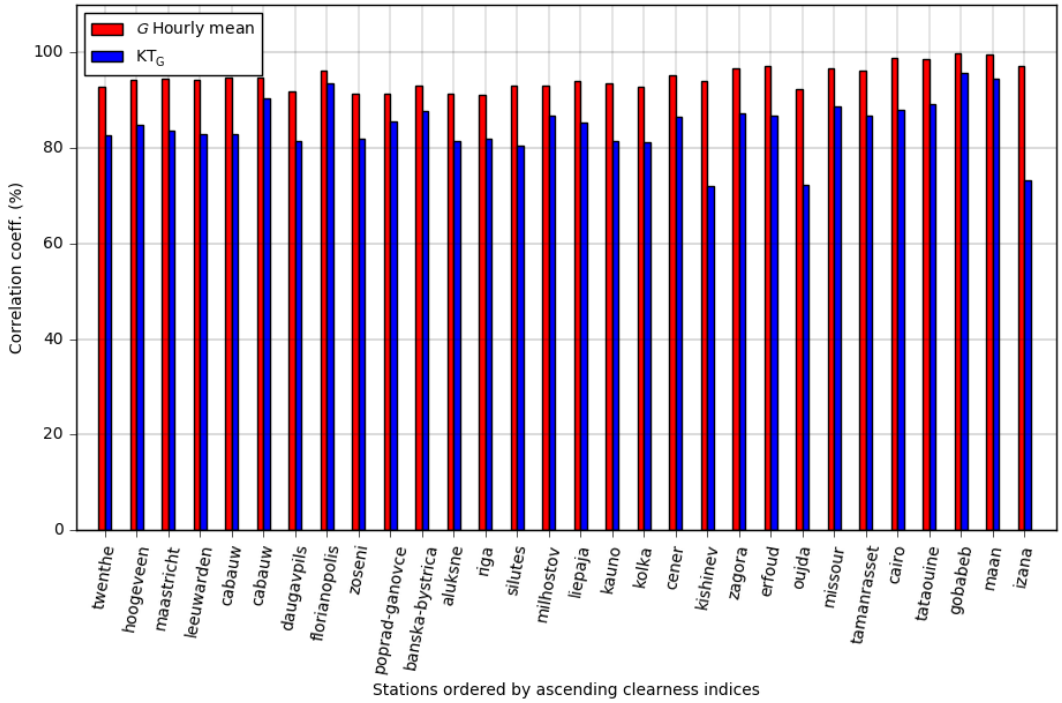

Figure 3.4. Correlation coefficients for global irradiance and clearness index.

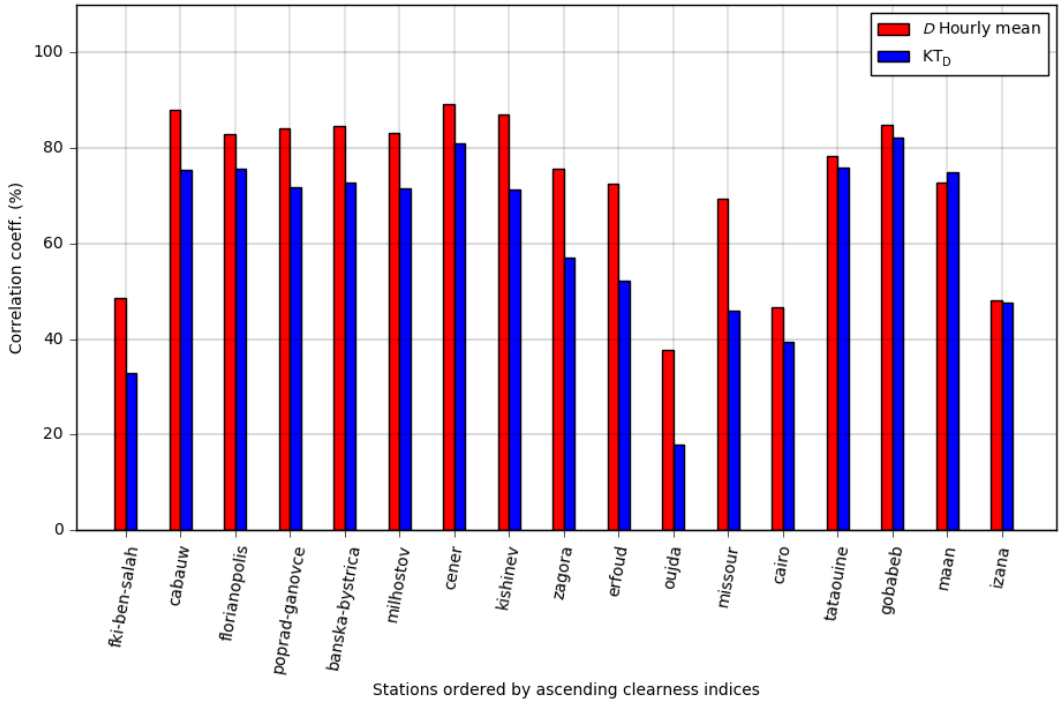

Figure 3.5. Correlation coefficients for diffuse irradiance and clearness index.

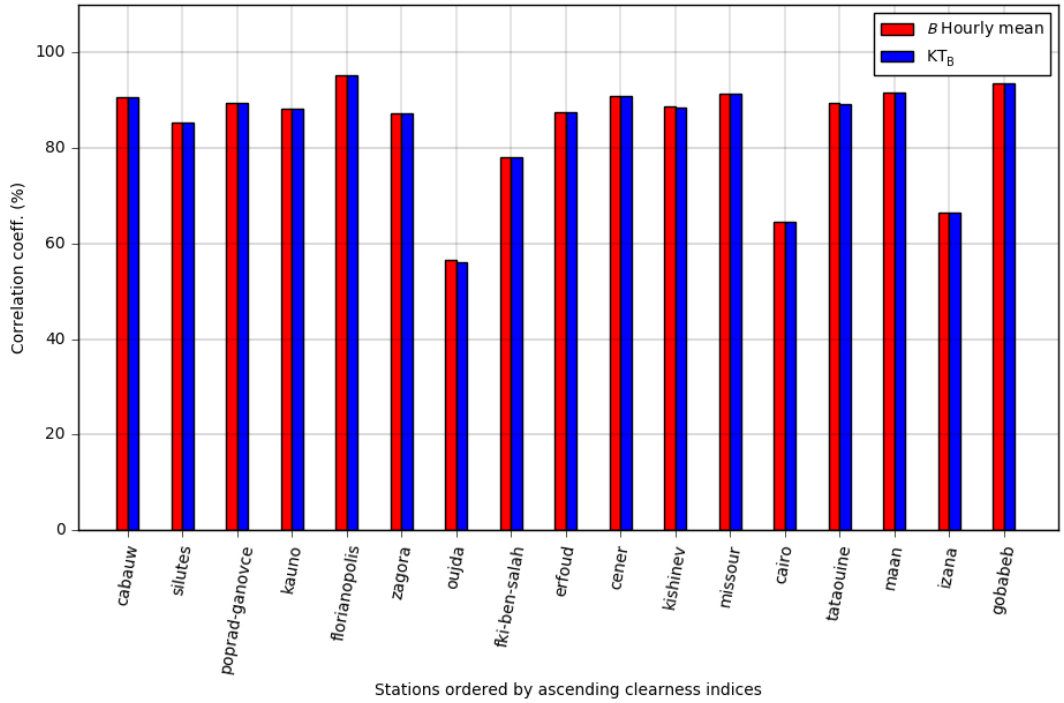

Figure 3.6. Correlation coefficients for direct normal irradiance and clearness index.

3.3 Ability to reproduce the frequency distributions of measurements

The frequency distributions of G and KT_G (Fig. 3.7 and 3.8), D and KT_D (Fig. 3.9 and 3.10), B and KT_B (Fig. 3.11 and 3.12) are given for several classes of irradiances or *KT*. The objective of these figures is to display in which bins of values an over- or underestimation of the frequencies may be observed.

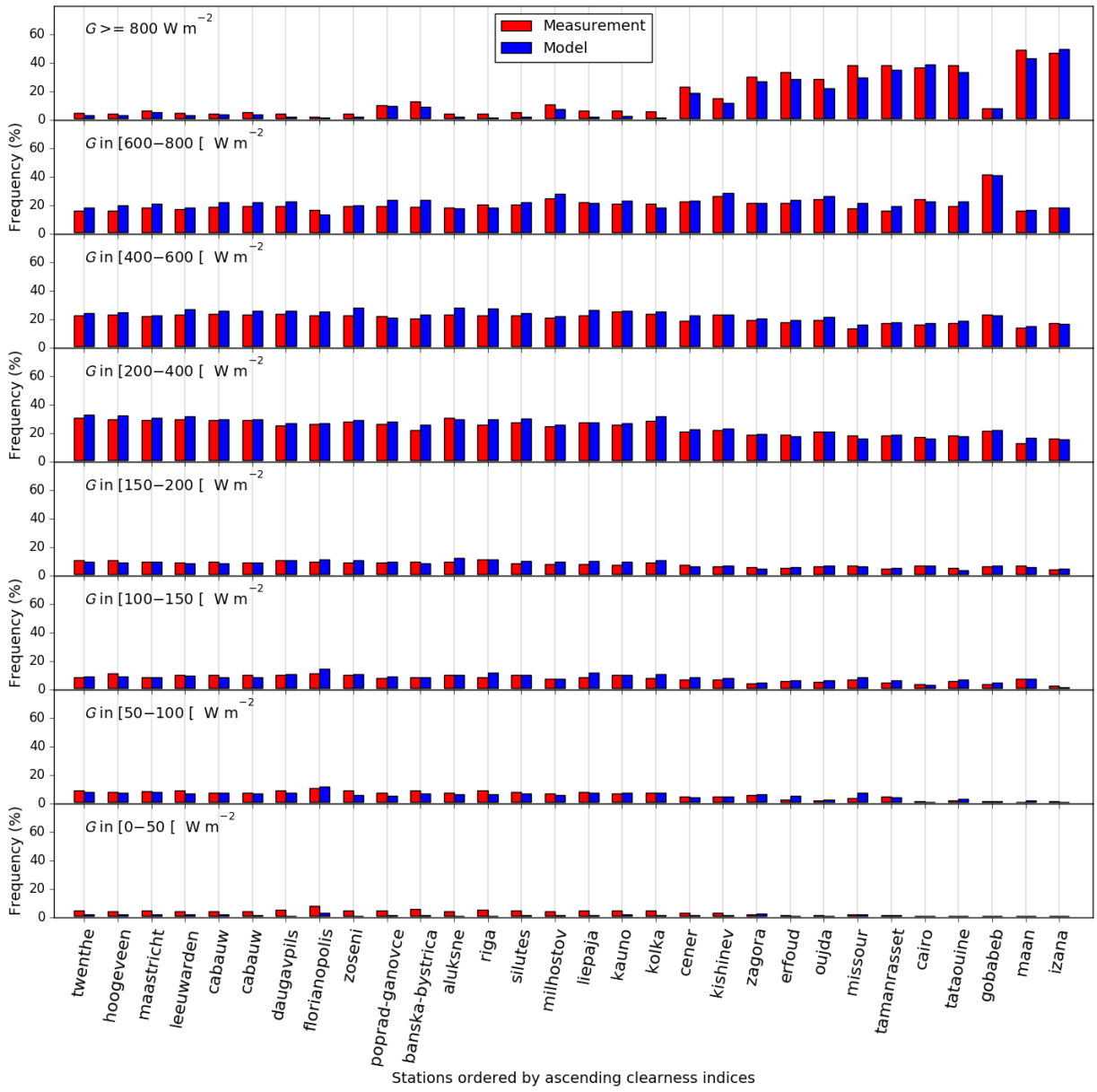

Figure 3.7. Frequency distribution of measurements for global irradiance.

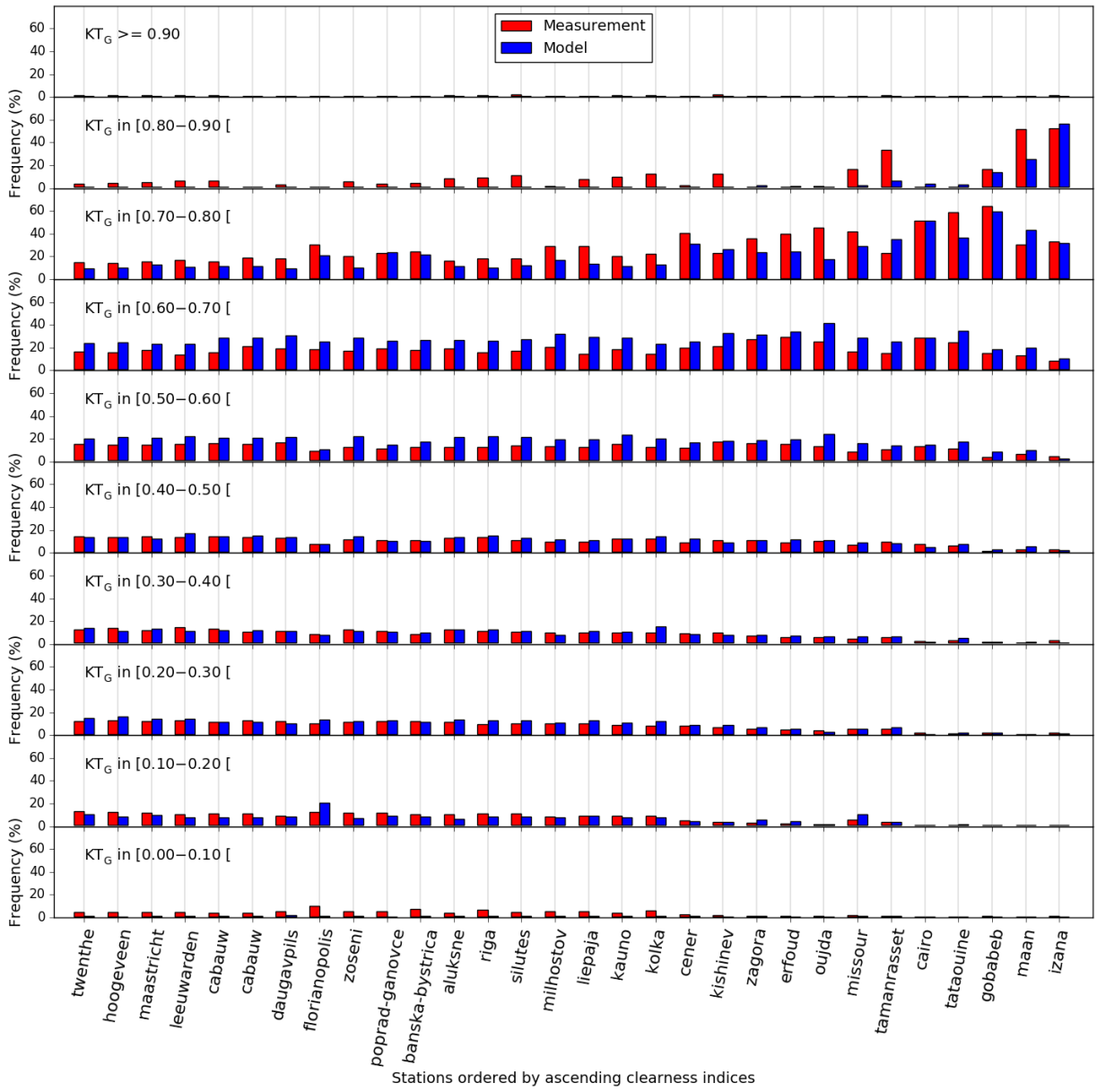

Figure 3.8. Frequency distribution of measurements for global clearness index.

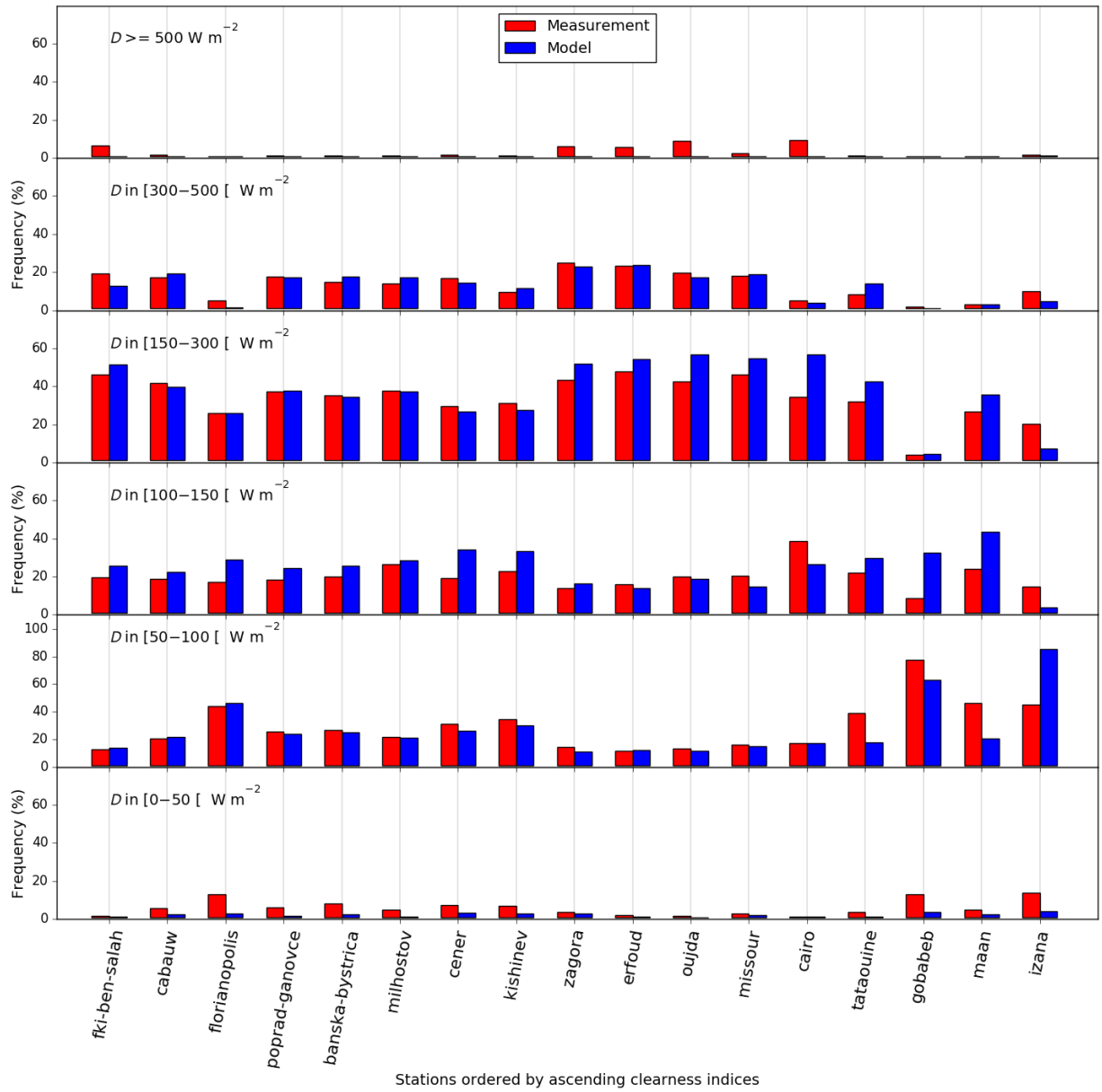

Figure 3.9. Frequency distribution of measurements for diffuse irradiances.

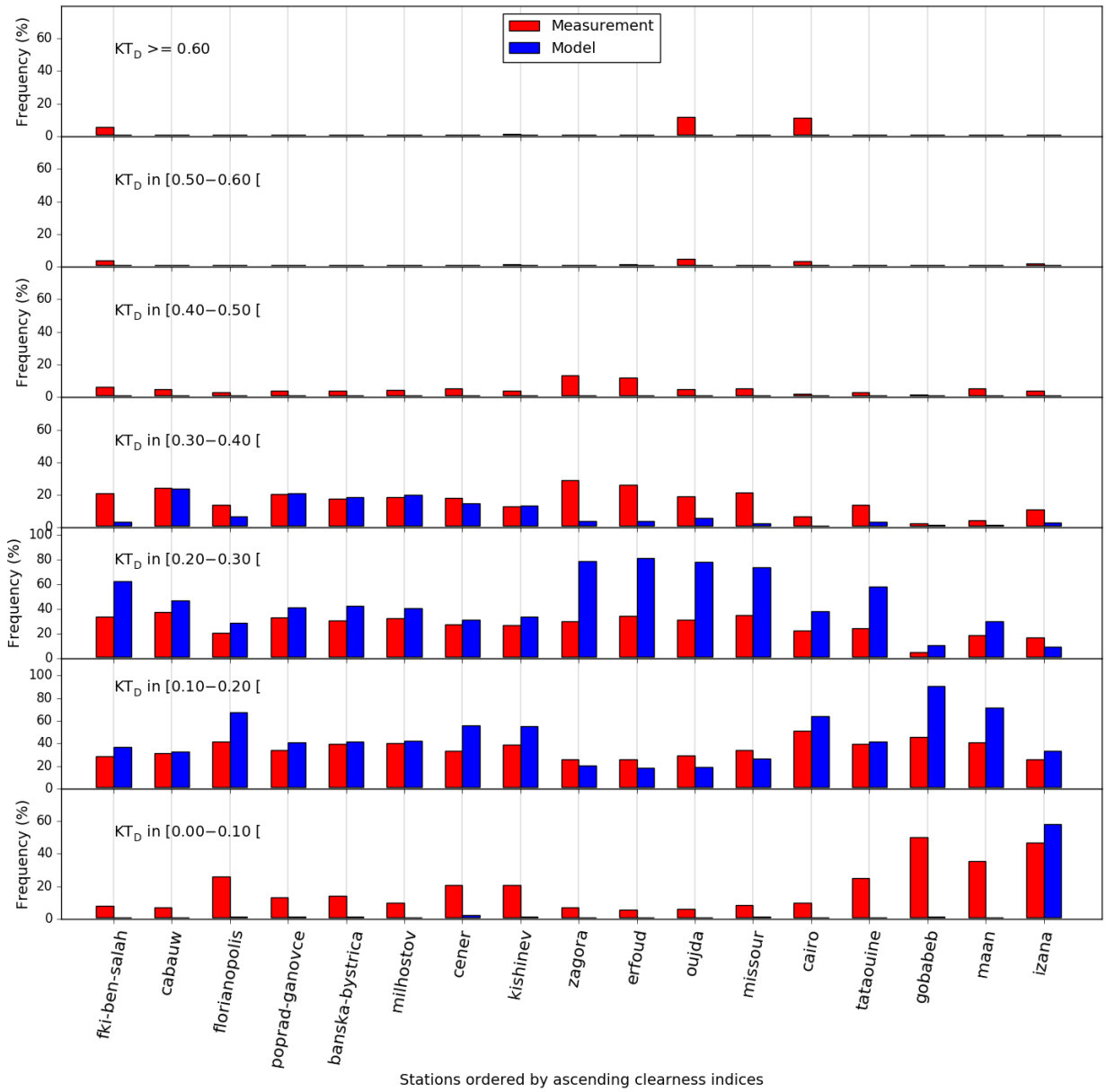

Figure 3.10. Frequency distribution of measurements for diffuse clearness index.

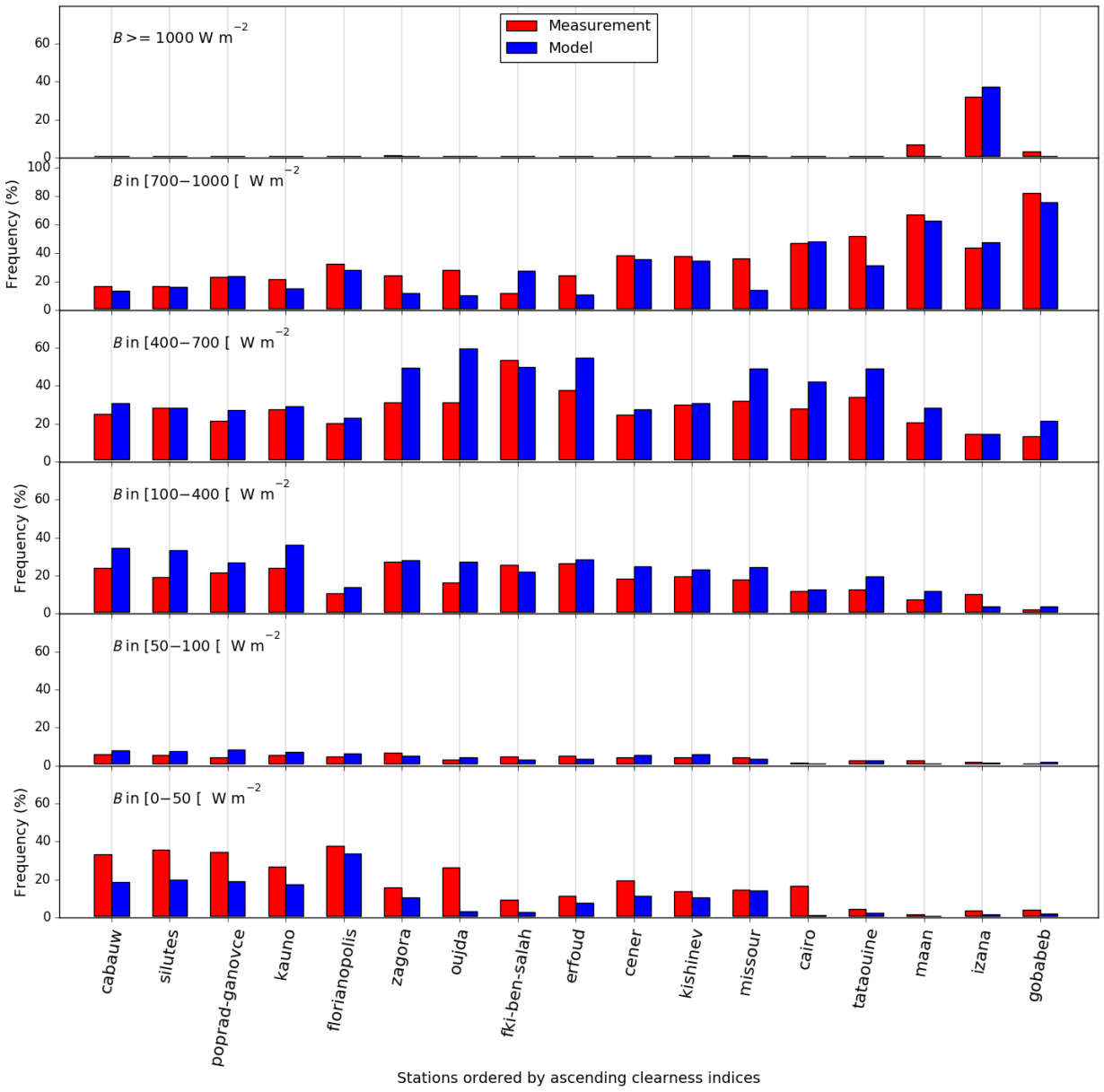

Figure 3.11. Frequency distribution of measurements for direct irradiances

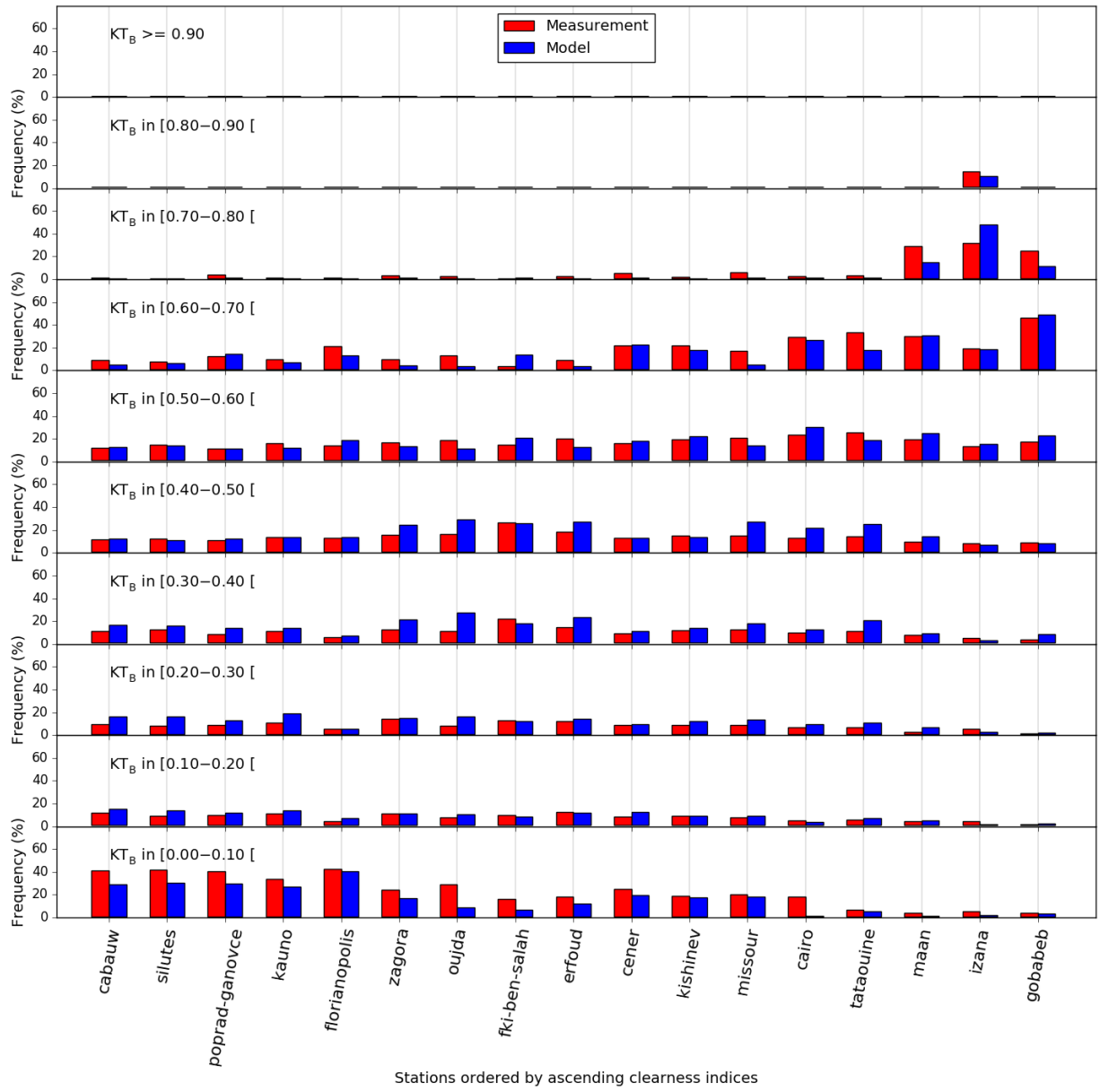

Figure 3.12. Frequency distribution of measurements for direct clearness index.

3.4 Ability to reproduce the monthly means and standard deviation for the period

The final batch of analyses deals with the capability of CRS to reproduce the monthly means of the irradiance for each month of the period and its variability within a month, expressed as the standard-deviation of the hourly values (estimates and observations) within this month. Figures 3.13 to 3.15 are respectively for *G*, *D* and *B*.

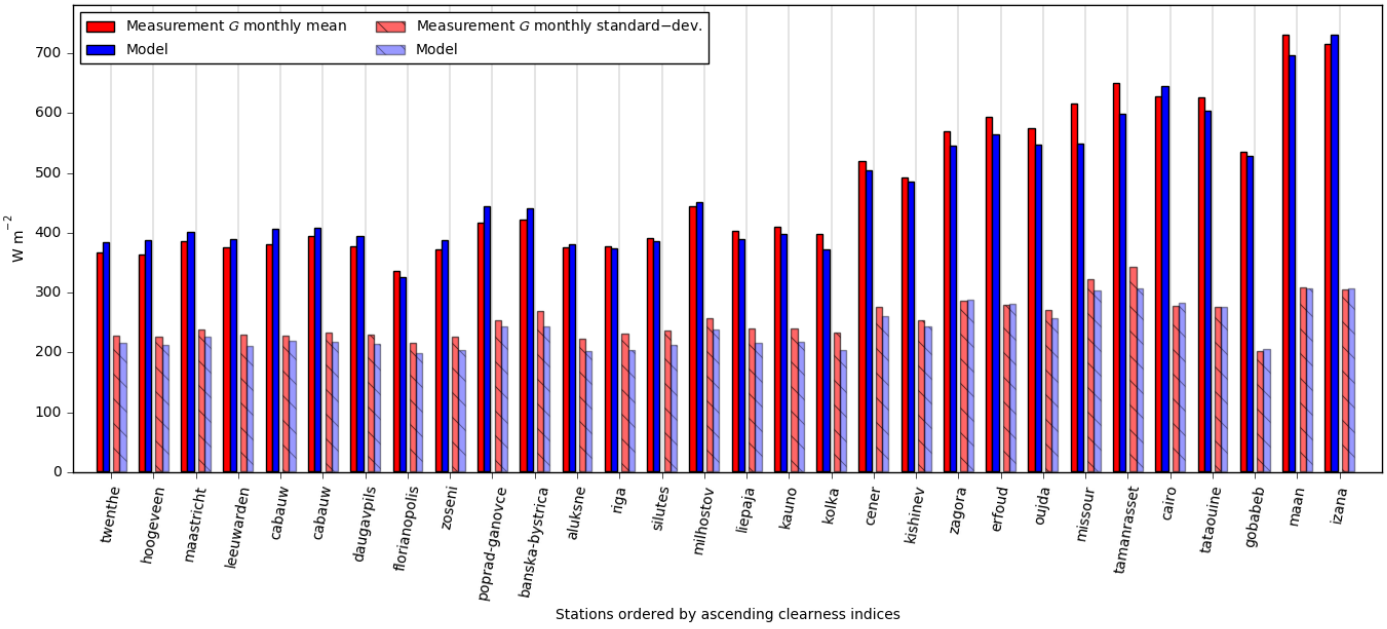

Figure 3.13. Monthly means and standard-deviations for global irradiance.

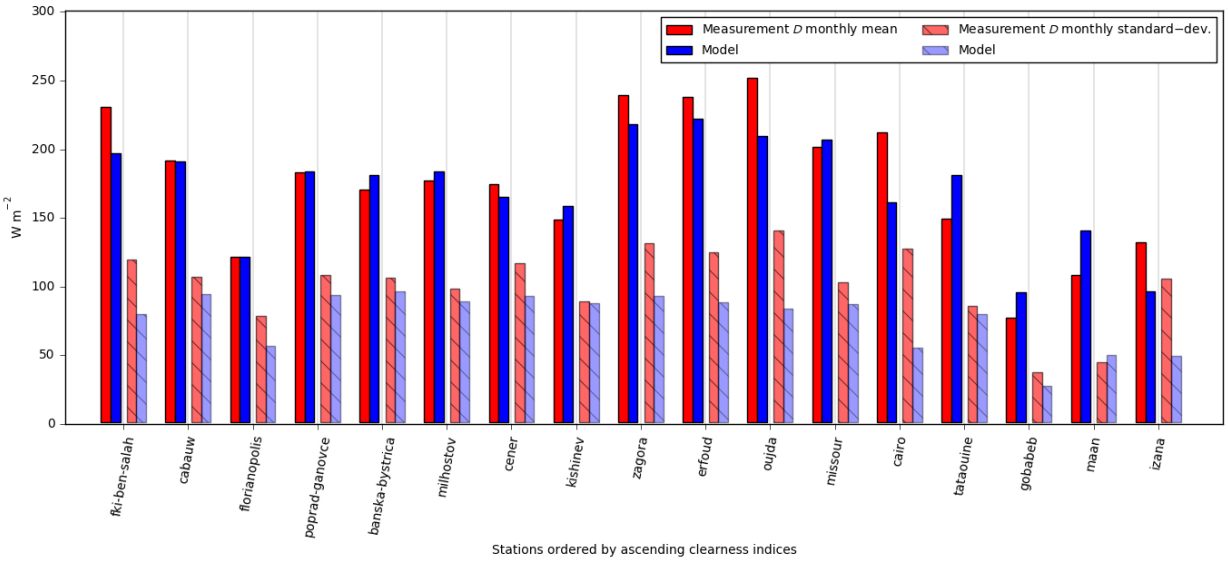

Figure 3.14. Monthly means and standard-deviations for diffuse irradiance.

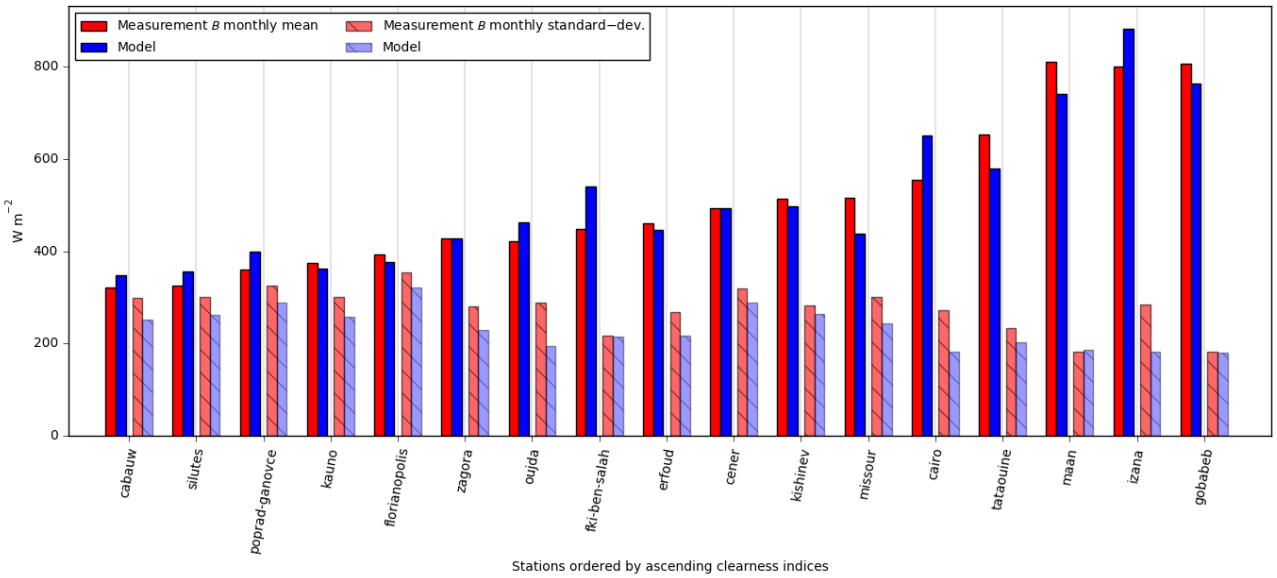

Figure 3.15. Monthly means and standard-deviation for direct normal irradiance.

3.5 Multi-annual statistical indicators

Statistical indicators (mean irradiance, mean KT, relative bias and relative RMSE) have been computed for the JJA period and for the years 2016 to 2020. Figures 3.16 to 3.18 are respectively for *G*, *D* and *B*.

3.5.1 Global irradiance

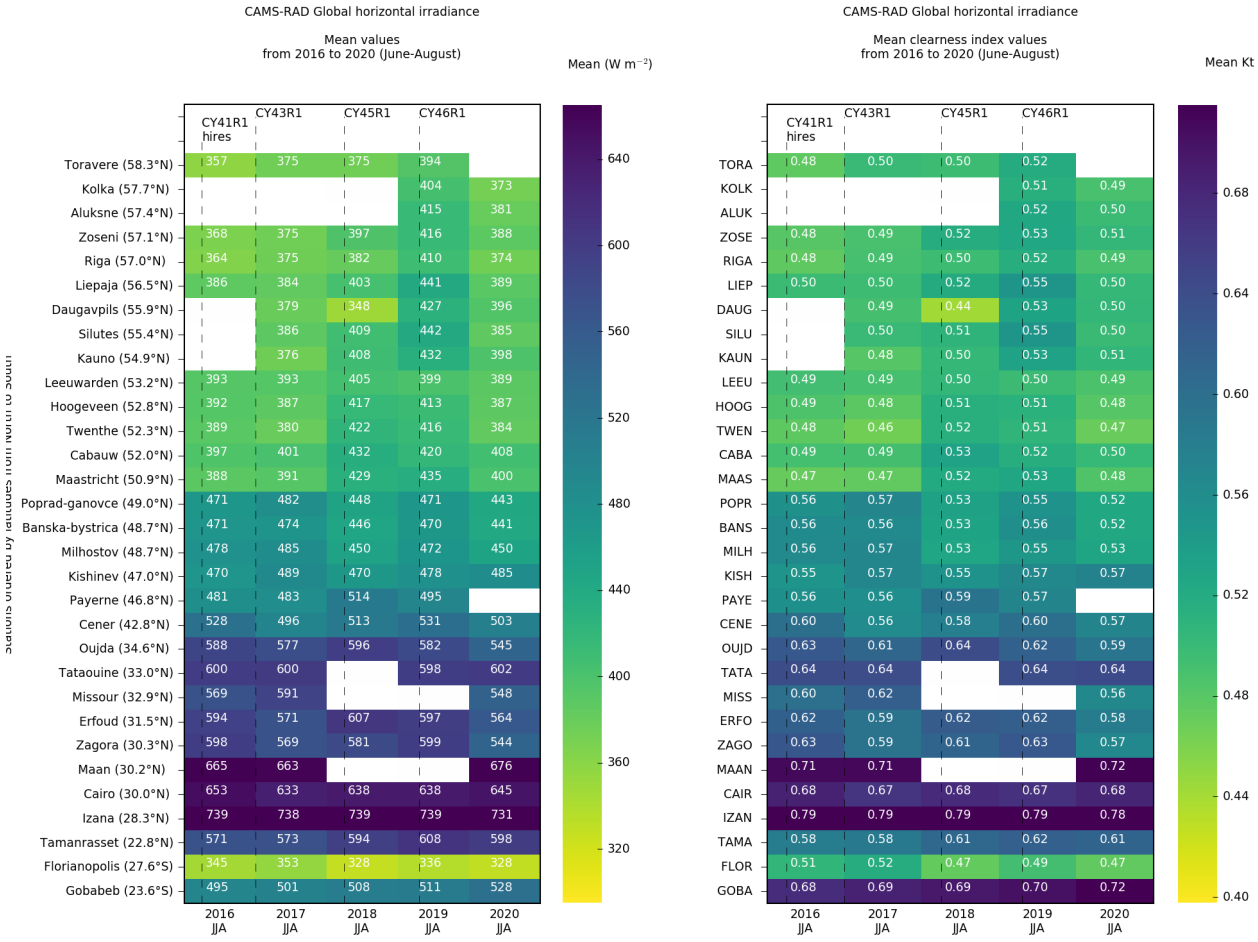

Figure 3.16a. Multi-annual means for CAMS-RAD global horizontal irradiance (left) and clearness index (right) JJA quarter from 2016 to 2020.

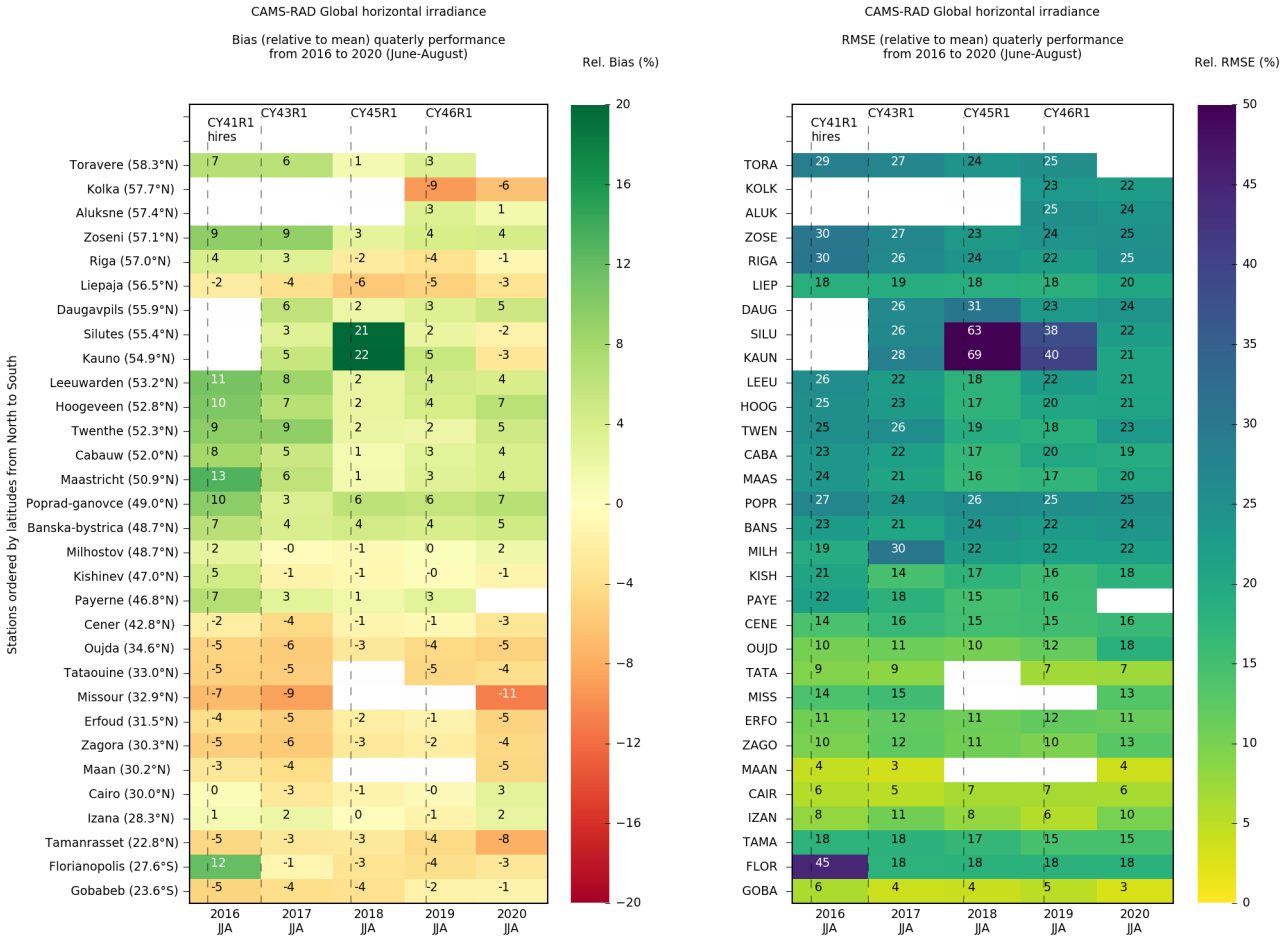

Figure 3.16b. Multi-annual relative bias (left) and relative RMSE (right) for CAMS-RAD global horizontal irradiance JJA quarter from 2016 to 2020.

3.5.2 Diffuse irradiance

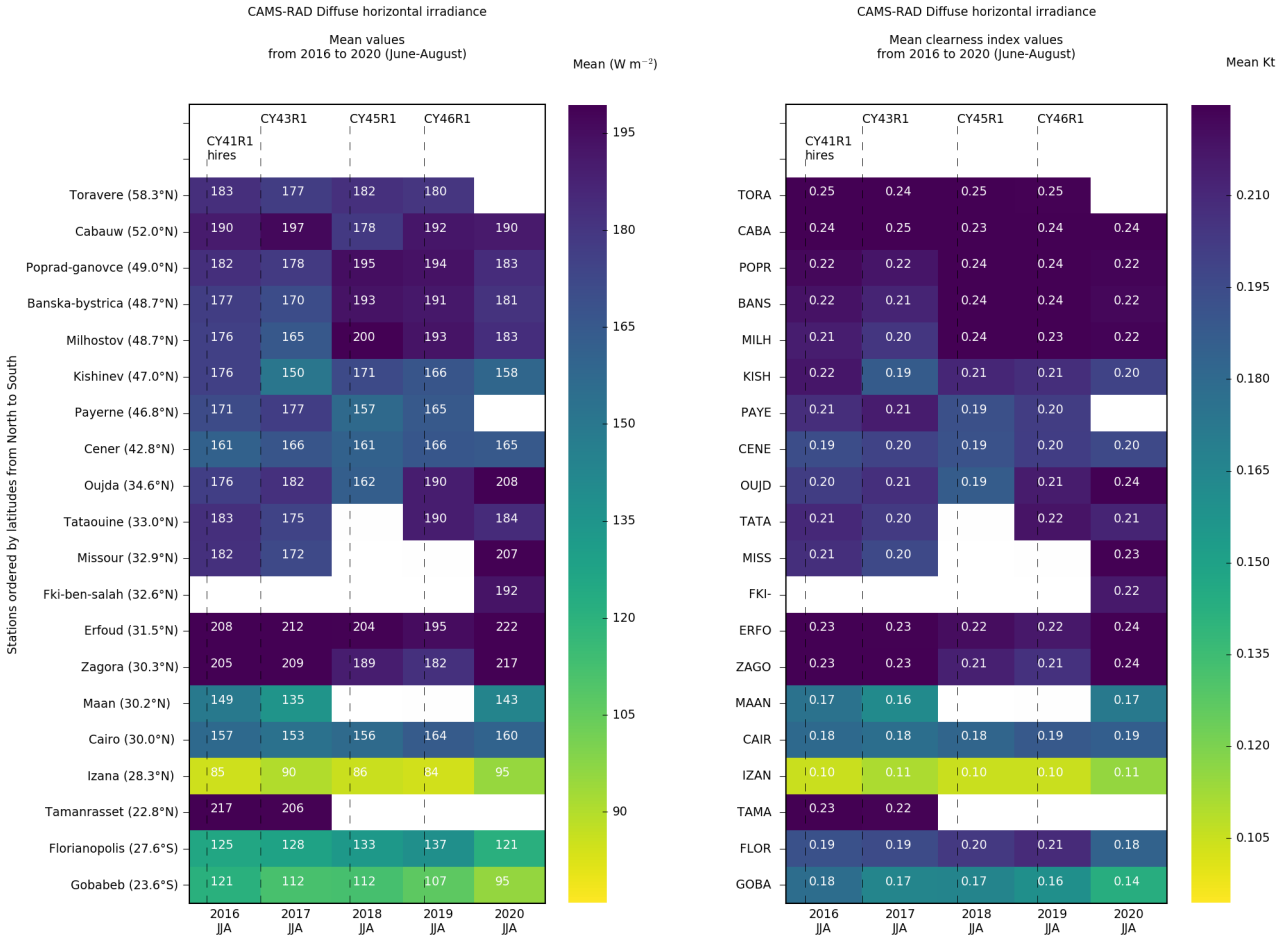

Figure 3.17a. Multi-annual means for CAMS-RAD diffuse horizontal irradiance (left) and clearness index (right) JJA quarter from 2016 to 2020.

Figure 3.17b. Multi-annual relative bias (left) and relative RMSE (right) for CAMS-RAD diffuse horizontal irradiance.
JJA quarter from 2016 to 2020.

3.5.3 Direct normal irradiance

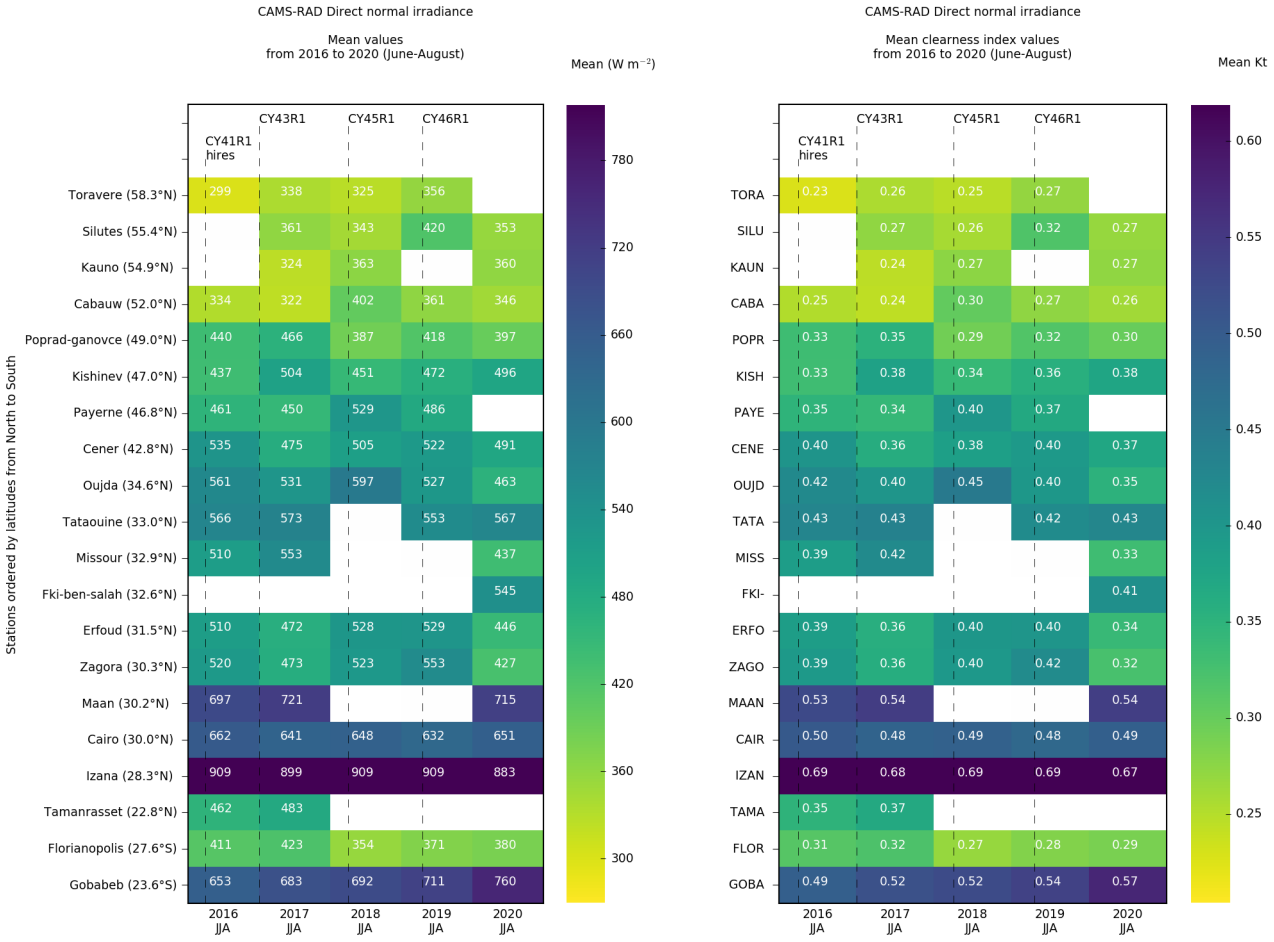

Figure 3.18a. Multi-annual means for CAMS-RAD direct normal irradiance (left) and clearness index (right) JJA quarter from 2016 to 2020.

Figure 3.18b. Multi-annual relative bias (left) and relative RMSE (right) for CAMS-RAD direct normal irradiance JJA quarter from 2016 to 2020.

3.6 Recommendations

As already reported in previous reports, there is room to improve the CRS for large solar zenithal angles. There are several cases with large *B* values observed in the ground observations which are underestimated in CRS. The cloud analysis from Meteosat images indicates a fully cloudy pixel with cloud coverage of 100 % and a low cloud optical depth. In the current scheme the cloud optical depth is set to a clipping value of 0.5 even if the retrieval provides a smaller value. This was a meaningful setting for the original application field of the used cloud retrieval package, but is not appropriate for surface radiation calculations. The exact value of the cloud optical depth plays a greater role when the sun is low above horizon which happens very often in winter at great

latitude, and at the beginning and end of the day in any case. This clipping value will be removed in the next version of the cloud retrieval package.

The CRS is composed of two models (see https://atmosphere.copernicus.eu/solar-radiation and the User Guide published there). The sky model of the CRS - called McClear - exploits the CAMS service information on aerosol properties and total column content in water vapour and ozone. It provides irradiances that would be observed in cloud-free conditions. McClear generally performs well as shown by several publications (Eissa et al., 2015; Lefèvre et al., 2013, Lefèvre, Wald, 2016; Marchand et al., 2017). However, detailed analyses of the deviations for CRS reveal discrepancies that may be large also for cloud-free cases. These discrepancies may be traced back to the over- or underestimation of the occurrences of cloud-free cases or to any gross errors in aerosol conditions modelled as input to McClear. Note should be taken that there is no means in this study to discriminate the cases of underestimation of the occurrences of overcast cases and those of underestimation of the optical depth. Both cases appear as an underestimation by CRS of the frequency of low clearness indices. Similarly, there is no means to discriminate the cases of overestimation of the occurrences of medium skies cases and those of underestimation of the optical depth of the optically thick clouds or overestimation of the optical depth of the optically thin clouds. These cases appear as an overestimation by CRS of the frequency of medium clearness indices. Finally, there is no means to discriminate the cases of underestimation of the occurrences of cloud-free cases and those of overestimation of the optical depth of the optically thin clouds. These cases appear as an underestimation by CRS of the frequency of large clearness indices.

4 Sources of data

Measurements are taken from various sources and measuring stations that are discussed in this section. Note that a more detailed presentation is done in the ground measurement catalogue updated every year: CAMS72_2018SC2_D72.1.4.1-2020_ground_catalogue_202012.pdf for December 2020.

4.1 Sources of data

Efforts are made to build the quarterly validation reports with the same set of stations to better follow and monitor the quality of the irradiance products delivered by the CRS, though this is difficult as discussed later.

Measurements originate from different networks as reported in Table 4.1. They have been acquired in different time systems (UT: Universal Time, TST: True Solar Time, GMT: Greenwich Meridian Time). No change in time system is performed during this validation. The handling of the different time systems is described in the annex A describing the procedure for validation.

Table 4.1. Source of data for each station, time system and type of data (*G, B, D* stands respectively for global, direct at normal incidence and diffuse), ordered from North to South.

Station	Source of data	Time system	Initial summarization	Type of data acquired
Toravere	BSRN	UT	1 min	G B D
Aluksne	Latvian Environment, Geology and Meteorology Centre (LEGMC)	TST	1 h	G - -
Kolka				G - -
Dobele				G B -
Riga				G - -
Zoseni				G - -
Liepaja				G - -
Rucava				G - -
Daugavpils				G - -
Silutes	Lithuanian Hydrometeorological Service (LHMS)	UT	1 h	G B -
Kauno				
Leeuwarden	KNMI	UT	1 h	G - -
Hoogeveen				
Twenthe				
Maastricht				
Cabauw	BSRN	UT	1 min	G B D
Poprad-Ganovce	Slovak Hydrometeorological Institute (SHMI)	UT	1 min	G B D
Banska-Bystrica				G - D
Milhostov				G - D
Kishinev	WRDC	GMT+2	1 h	G B D
Payerne	BSRN	UT	1 min	G B D
Izaña	BSRN	UT	1 min	G B D
Oujda	EnerMENA	UT	1 min	G B D
Tataouine		UT+1		
Fki-Ben-Salah		UT		
Missour		UT		
Erfoud		UT		
Cairo		UT+2		
Zagora		UT		
Ma'an		UT+2		
Tamanrasset	BSRN	UT	1 min	G B D
Gobabeb				
Florianopolis				

4.2 Short description of the stations selected for the validation

The selected stations are located in Europe, Africa and South America (see maps in Figures 2.1 and 2.2). Their geographical coordinates are given in Table 4.2.

Table 4.2. List of stations used to realize the validation report in general, and their coordinates.

Country	Station	Latitude	Longitude	Elevation a.s.l. (m)
Estonia	Toravere	58.254	26.462	70
Latvia	Aluksne	57.440	27.035	197
Latvia	Kolka	57.743	22.584	30
Latvia	Zoseni	57.135	25.906	188
Latvia	Riga	56.951	24.116	6
Latvia	Dobele	56.620	23.320	42
Latvia	Liepaja	56.475	21.021	4
Latvia	Rucava	56.162	21.173	19
Latvia	Daugavpils	55.870	26.617	98
Lithuania	Silutes	55.352	21.447	5
Lithuania	Kauno	54.884	23.836	77
The Netherlands	Hoorn	53.393	5.346	0
The Netherlands	Leeuwarden	53.225	5.755	1
The Netherlands	Hoogeveen	52.750	6.575	16
The Netherlands	Twenthe	52.273	6.897	34
The Netherlands	Cabauw	51.972	4.927	-1
The Netherlands	Vlissingen	51.442	3.596	8
The Netherlands	Maastricht	50.906	5.762	114
United Kingdom	Camborne	50.217	-5.317	88
Slovakia	Poprad-Ganovce	49.035	20.324	709
Slovakia	Banska-Bystrica	48.734	19.117	427
Slovakia	Milhostov	48.663	21.722	105
Moldova	Kishinev	47.000	28.817	205
Switzerland	Payerne	46.815	9.944	491
France	Carpentras	44.083	5.059	100
Spain	PSA	37.091	-2.358	500
Spain	Izaña	28.309	-16.499	2373
Morocco	Oujda	34.650	-1.900	617
Morocco	Missour	32.860	-4.107	1107
Morocco	Fki-Ben-Salah	32.578	-6.622	485
Morocco	Erfoud	31.491	-4.218	859
Morocco	Zagora	30.272	-5.852	783
Egypt	Cairo	31.036	31.009	104
Tunisia	Tataouine	32.974	10.485	210
Jordan	Ma'an	30.172	35.818	1012
Algeria	Adrar	27.878	-0.270	262
Algeria	Tamanrasset	22.790	5.529	1385
Namibia	Gobabeb	-23.561	15.042	407
Brazil	Florianopolis	-27.605	-48.523	11

The selected stations are located in several different climates as reported in Table 4.3. The description of climates is taken from the updated world map of the Köppen-Geiger climate classification by Peel et al. (2007).

Table 4.3. List of climates and corresponding stations

Climate	Stations
Dfa: Continental wet. Cold climate without dry season and hot summer	Poprad-Ganovce, Banska-Bystrica, Milhostov
Dfb: Continental wet. Cold climate without dry season and warm summer	Toravere, Zoseni, Riga, Dobele, Daugavpils, Liepaja, Aluksne, Kolka, Rucava, Silutes, Kauno, Kishinev
Cfa: Temperate climate without dry season and hot summer	Florianopolis
Cfb: Temperate climate without dry season and warm summer	Hoorn, Hoogeveen, Twenthe, Cabauw, Leeuwarden, Maastricht, Vlissingen, Camborne, Payerne
Csa: Temperate climate with dry and hot summer	Oujda, Missour
Csb: Temperate climate with dry and warm summer (Mediterran climate)	Carpentras, PSA, Izaña
BWh: Arid and hot climate of desert type	Tataouine, Erfoud, Cairo, Zagora, Ma'an, Tamanrasset, Fki-Ben-Salah
BWk: Arid and cold climate of desert type	Gobabeb

Among the set of stations, are several stations, such as Toravere, which are at the edge of the field of view of the Meteosat Second Generation satellites and most likely at the edge of physical assumptions used when retrieving cloud properties. This validation is meant to include extreme cases into the station list.

One may note that though the validation aims at validating the variables *G*, *B*, and *D* delivered by the CRS, several stations are included that measure only the global irradiance *G*. They have been selected in order to check the spatial consistency of the quality of the CRS products within the same network and same climate. Figure 2.1 shows several groups of stations that are close to each other within the same climate: The Eastern Baltic area, The Netherlands, and Slovakia. One expects similar performances of CRS within a group.

It should be underlined that the validation process cannot be automated in its present form. Hence, the number of selected stations and the choice of these stations is a trade-off between the desire to cover as much as possible various climatic conditions and the amount of human resources available.

4.3 Evolution of the list of stations

The selection of the stations considers the results published in scientific journals or conferences. Several authors have compared McClear or CRS estimates to ground-based measurements. These publications are analyzed to see if there are differences in quality when compared to our own validations.

The conclusions of these analyses may have an impact on the choice and the number of stations selected for the quarterly validation. For example, if one or more authors report performances that are dissimilar to ours in geographical areas for which we do not have stations, we will make our best to obtain measurements from stations if they obey our constraints in quality and timely access. In another example, authors may have made in-depth studies of the performances of CRS in geographical areas where we have stations, such as the Netherlands where we are using several KNMI stations. Given this background, exploiting a single KNMI station may be sufficient now to monitor the performances of CRS in this area.

4.4 Stations under evaluation

Some stations providing unusual observations are commented below.
From the #28 issue, some issues are not commented anymore. It concerns (see last #27 issue for details):

- The KNMI station of Hoorn was removed from the set used for the quarterly validation. This station will be reported in the next ground data catalogue for information and as a warning to users at the coastal limit.
- The enerMENA station of Missour which gave abnormal overestimated measurements of diffuse irradiances during April and June 2018. This station was under maintenance since then and resume on October 2019.

From this #31 issue, some other stations are not commented anymore (see last #30 issue for details):

- The Lithuanian stations of Silutes and Kauno. Thanks to the renovation operated in January 2020, problems have been solved, included many times shifts.

Still under evaluation are stations Zagora, Erfoud and Oujda in Morocco, Cairo in Egypt. Some discrepancies between estimated CRS and measurements have been reported in previous reports.

4.4.1 Cairo (Egypt)

During the past 2019 JJA quarter some bad values for the *D* component appeared at Cairo which were not eliminated with the quality check process. A manual elimination of the problematic days had to be done. Figure 4.1 presents the times-series before and after this elimination.
In the meantime, it appears that the MESOR source format of the ground data were changed i.e. the flag32 “irradiance data inaccurate” used for data filtering moved to a column to another. Once

corrected (and without manual elimination) results return to better values although a peak in August 2018 remains (Fig. 4.2).
The issue concerning the structure of the ground data files and the difficulty to eliminate suspicious data has been returned to the EnerMENA team at Almeria. They are working to provide a new structure which will make the extraction easier and safer. This new structure has been received in November 2020 for the July-Sept. 2020 dataset.
During the present JJA 2020 period, contrary to the global irradiance, the diffuse and direct irradiances present very large variations in June (Fig. 4.3). A tracker failure until 18 of June along with a lack of cleaning during failure period explain these anomalies.

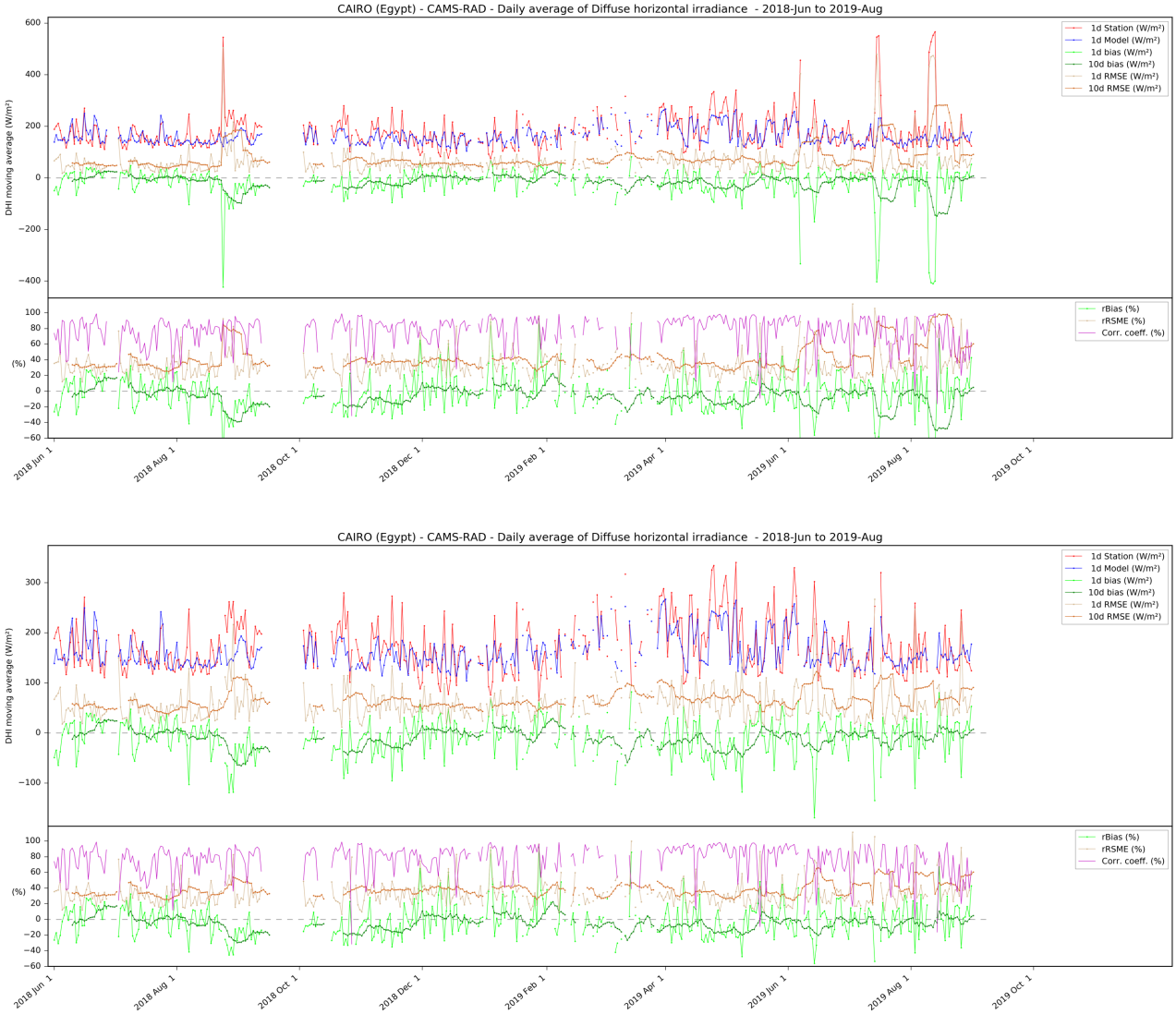

Figure 4.1. Station Cairo, daily and 10 days running average of diffuse irradiance from June 2018 to August 2019. Top: with the station data source (without correction on the MESOR format). Bottom: after elimination of visually defined problematic days.

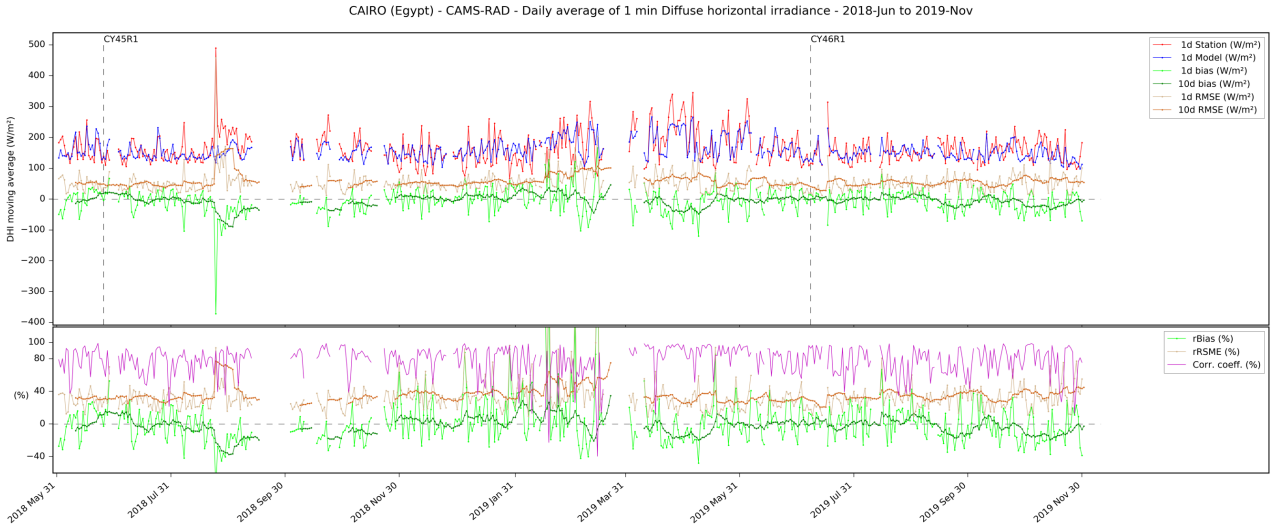

Figure 4.2. Station Cairo, daily and 10 days running average of diffuse irradiance from June 2018 to November 2019, after correction of the MESOR source format (without manual elimination).

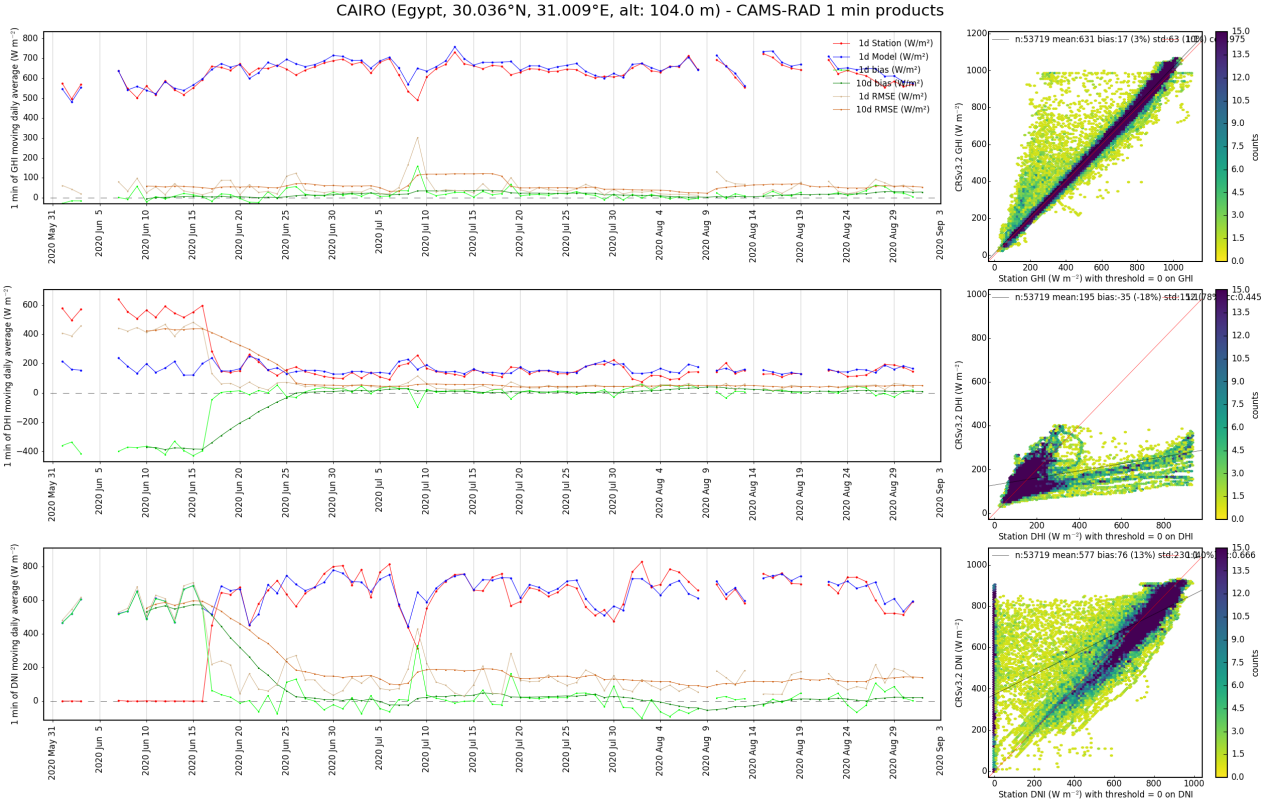

Figure 4.3. Station Cairo, daily and 10 days running average of irradiance, during JJA 2020.
Top: Global. Middle: Diffuse. Bottom: Direct normal irradiance.

4.4.2 Zagora (Morocco)

Zagora observes a sudden decrease in mid-January 2020 on *G* and *D* (Fig. 4.4). That creates a discrepancy between measured and estimated *G* from mid-January to July. On the contrary, it removes the discrepancy for *B* on the same period. Actually, the RSI sensor has been exchanged in January 2020. A new calibration has been applied that corrects the in-situ *G* component (Fig. 4.5). Nevertheless, *B* which is calculated from *G* and *D*, presents since then and until mid-June 2020 a discrepancy with estimated CRS that was not observed before.

Although large discrepancies appear during this JJA 2020 period for the *D* component, no problem was reported regarding the maintenance of in-situ sensors. Thus, the data have not been eliminated from the JJA 2020 dataset.

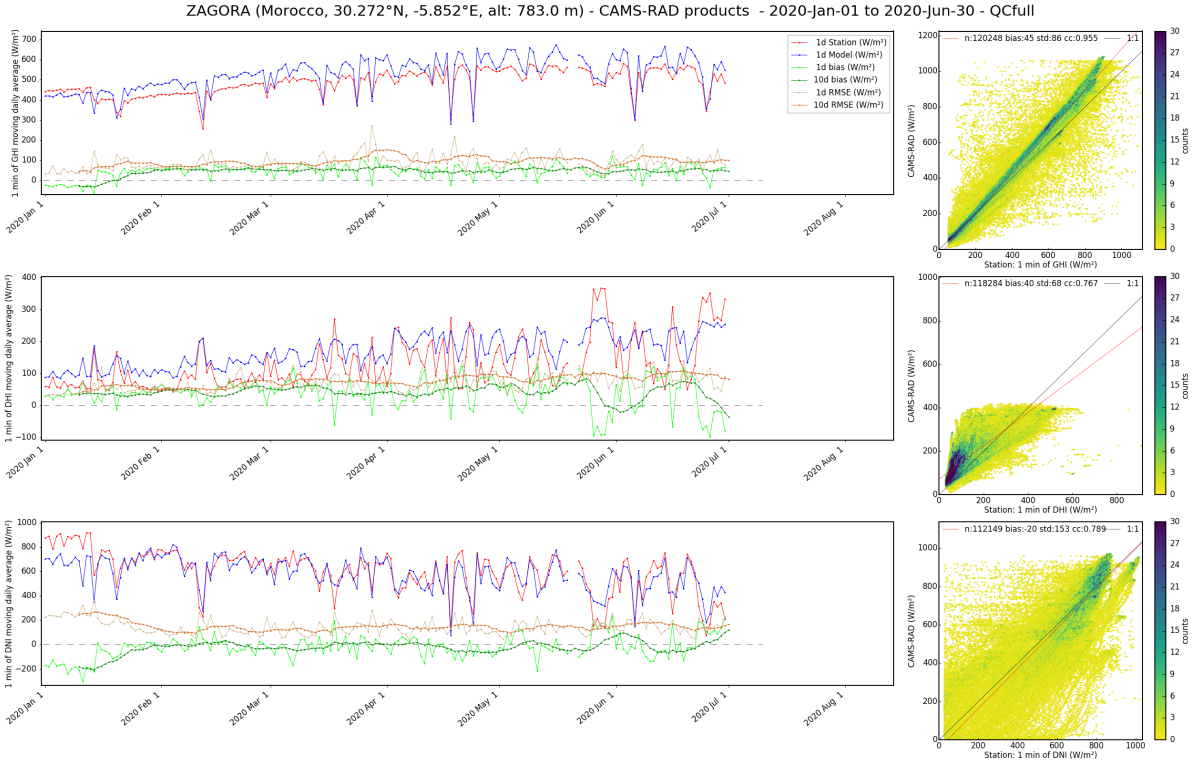

Figure 4.4. Station Zagora, daily and 10 days running average of irradiance from January to July 2020 (data source before correction of the calibration) Top: Global. Middle: Diffuse. Bottom: Direct normal irradiance

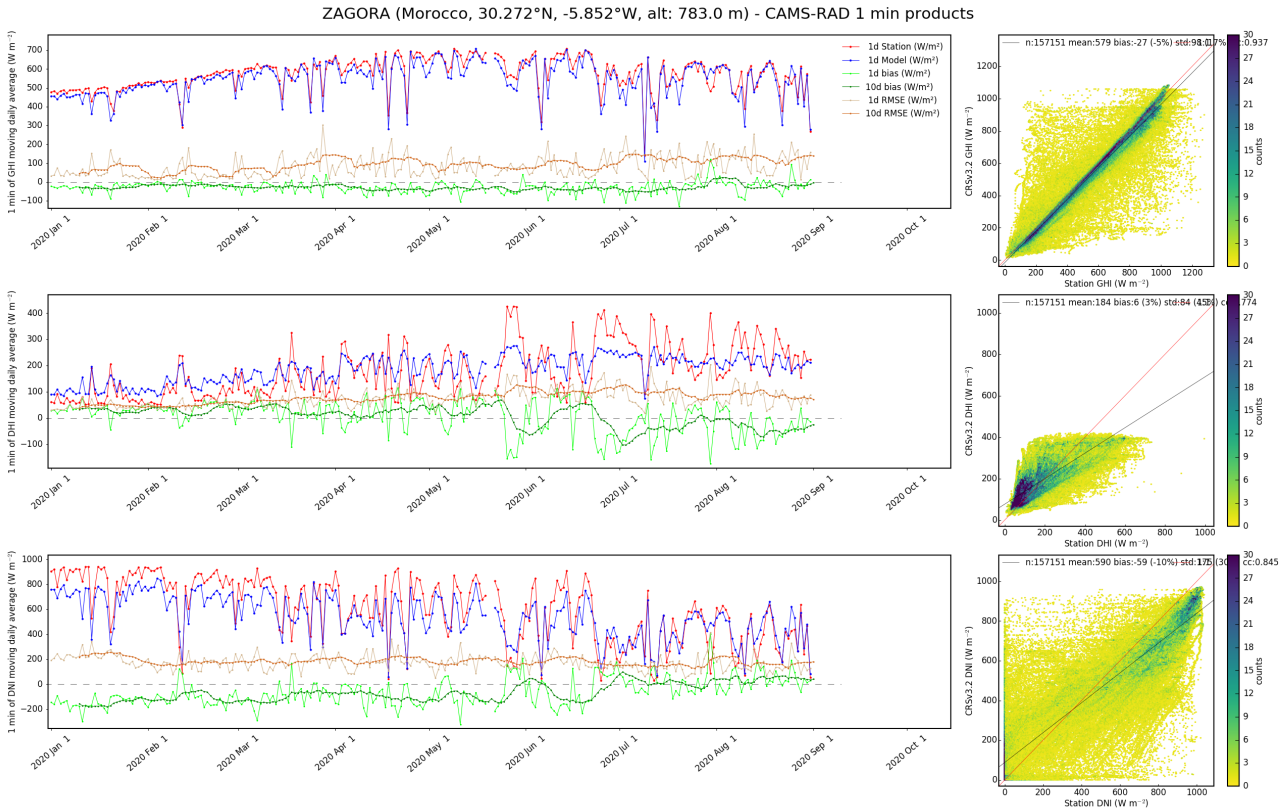

Figure 4.5. Station Zagora, daily and 10 days running average of irradiance from January to August 2020 (data source after correction of the calibration). Top: Global. Middle: Diffuse. Bottom: Direct normal irradiance.

4.4.3 Erfoud (Morocco)

The station Erfoud presents a decrease of *D* measurements from October 2019 to March 2020 and a sudden increase since then, with a concomitant variation of *B* in opposite way (Fig. 4.6). In this case of Erfoud, a remote site without regular cleaning, the continuously increasing deviations have been caused by dirt on the RSI sensor.

Although large discrepancies appear during this JJA 2020 period for the *D* component, no problem was reported regarding the maintenance of in-situ sensors. Thus, the data have not been eliminated from the JJA 2020 dataset.

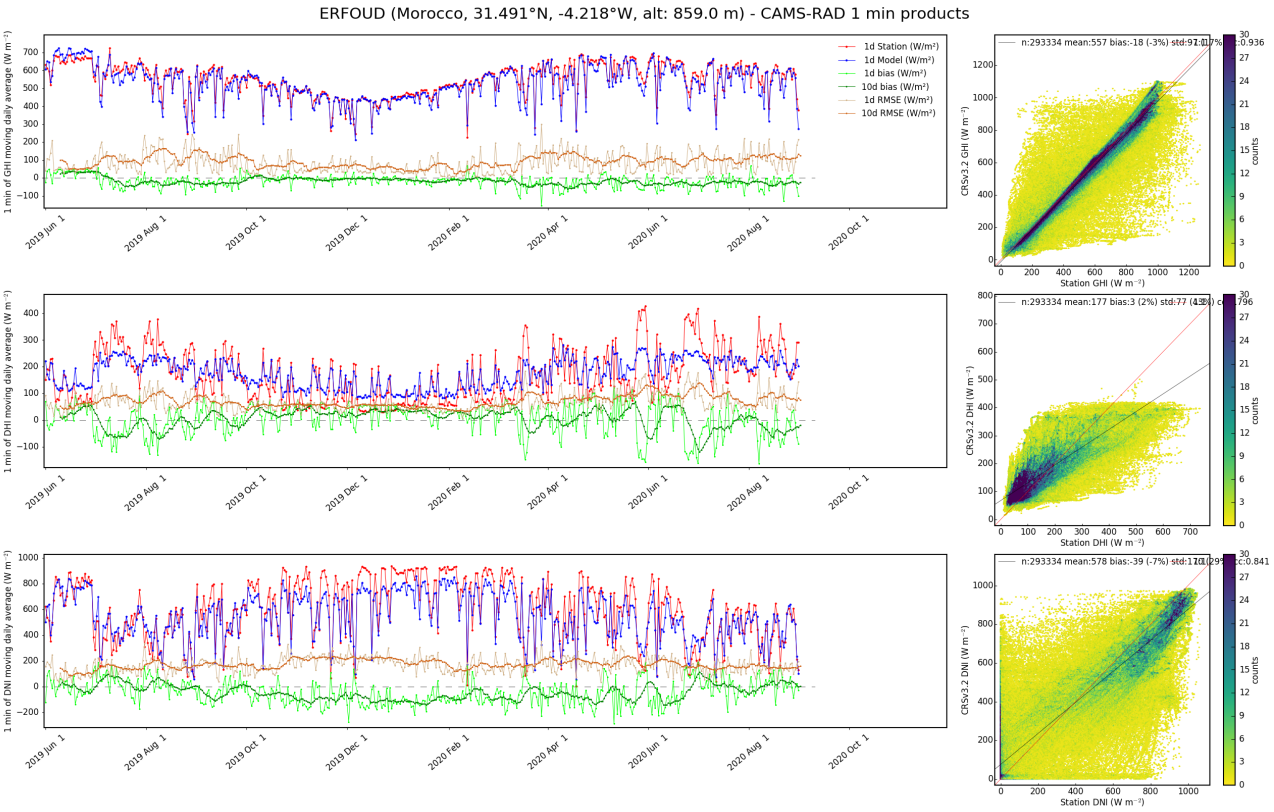

Figure 4.6. Station Erfoud, daily and 10 days running average of clearness index, from JJA 2019 to JJA 2020. Top: Global. Middle: Diffuse. Bottom: Direct normal clearness index.

4.4.4 Oujda (Morocco)

The station Oujda observes a sudden decrease of *G* in August 2019 (Fig. 4.7). In this case, one of the pyranometers may be not well levelled since the new calibration in August 2019.
Sensors were not cleaned during COVID-19 from March to May 2020, and a tracker failure occurred between 24 April and 3 May, and between 8-16 June which probably causes the discrepancy observed. No problem was reported for July 2020 although discrepancies remain. We have eliminated these dates from the dataset for the validation. Thus, the data have not been eliminated from the JJA 2020 dataset.

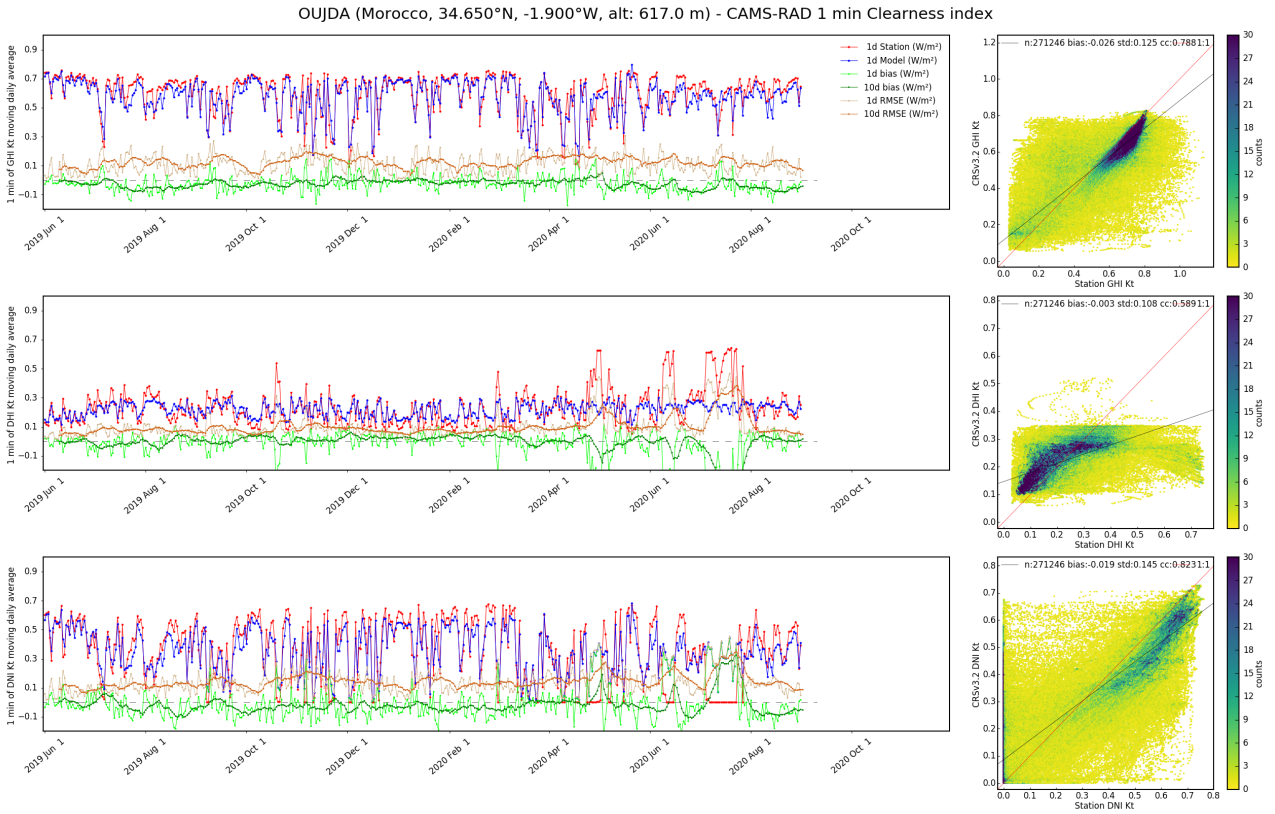

Figure 4.7. Station Oujda, daily and 10 days running average of clearness index, from JJA 2019 to JJA 2020. Top: Global. Middle: Diffuse. Bottom: Direct normal clearness index.

5 Acknowledgements

The authors recognize the key role of the operators of ground stations in offering measurements of solar radiation for this validation. The authors thank all ground station operators of the Baseline Surface Radiation Network (BSRN) for their valuable measurements and the Alfred Wegener Institute for hosting the BSRN website. They also thank the Global Atmosphere Watch (GAW) program of the World Meteorological Organization (WMO) and the World Radiation Data Center (WRDC) a laboratory of the Voeikov Main Geophysical Observatory in Saint-Petersburg, Russia, for hosting the GAW website. The authors thank the University of Jordan, CRTEn and IRESEN for operating the stations of respectively Ma'an, Tataouine and Missour that belong to the EnerMENA Network as well as the German aerospace center DLR for graciously making the measurements available, and Natalie Hanrieder for her precious information on station performance. The EnerMENA has been set up with an initial support of the German Foreign Office. The Latvian Environment, Geology and Meteorology Centre (LEGMC) and the Slovak Hydrometeorological Institute (SHMI) have kindly supplied measurements for respectively Latvia and Slovakia. The authors thank Alexandr A. Aculinin and his Atmospheric Research Group at the Institute of Applied

Physics of the Academy of Sciences of Moldova for generously providing the measurements at Kishinev. Measurements for The Netherlands have been downloaded from the web site of the KNMI.

6 Reference documents

Blanc, P., Wald, L.: The SG2 algorithm for a fast and accurate computation of the position of the Sun. Solar Energy, 86, 3072-3083, doi: 10.1016/j.solener.2012.07.018, 2012.

Blanc, P., Espinar, B., Geuder, N., Gueymard, C., Meyer, R., Pitz-Paal, R., Reinhardt, B., Renne, D., Sengupta, M., Wald, L., Wilbert, S.: Direct normal irradiance related definitions and applications: the circumsolar issue. Solar Energy, 110, 561-577, doi: 10.1016/j.solener.2014.10.001, 2014.

Eissa, Y., Munawwar, S., Oumbe, A., Blanc, P., Ghedira, H., Wald, L., Bru, H., Goffe, D.: Validating surface downwelling solar irradiances estimated by the McClear model under cloud-free skies in the United Arab Emirates. Solar Energy, 114, 17-31, doi: 10.1016/j.solener.2015.01.017, 2015.

ISO Guide to the Expression of Uncertainty in Measurement: first edition, International Organization for Standardization, Geneva, Switzerland, 1995.

Greuell W., J. F. Meirink, and P. Wang (2013), Retrieval and validation of global, direct, and diffuse irradiance derived from SEVIRI satellite observations, J. Geophys. Res. Atmos., 118, 2340–2361, doi:10.1002/jgrd.50194.

Korany M., M. Boraiy, Y. Eissa, Y. Aoun, M. M. Abdel Wahab, S. C. Alfaro, P. Blanc, M. El-Metwally, H. Ghedira, K. Hungershoefer, Wald, L.: A database of multi-year (2004-2010) quality-assured surface solar hourly irradiation measurements for the Egyptian territory. Earth System Science Data, 8, 105-113, doi: 10.5194/essd-8-105-2016, 2016.

Lefèvre, M., Oumbe, A., Blanc, P., Espinar, B., Gschwind, B., Qu, Z., Wald, L., Schroedter-Homscheidt, M., Hoyer-Klick, C., Arola, A., Benedetti, A., Kaiser, J. W., Morcrette, J.-J.: McClear: a new model estimating downwelling solar radiation at ground level in clear-sky condition. Atmospheric Measurement Techniques, 6, 2403-2418, doi: 10.5194/amt-6-2403-2013, 2013.

Lefèvre, M., Wald, L.: Validation of the McClear clear-sky model in desert conditions with three stations in Israel. Advances in Science and Research, 13, 21-26, doi: 10.5194/asr-13-21-2016, 2016.

Marchand, M., Al-Azri, N., Ombe-Ndeffotsing, A., Wey, E., Wald, L.: Evaluating meso-scale change in performance of several databases of hourly surface irradiation in South-eastern Arabic Peninsula. Advances in Science and Research, 14, 7-15, doi:10.5194/asr-14-7-2017, 2017.

Peel, M. C., Finlayson, B. L., Mcmahon, T. A.: Updated world map of the Köppen-Geiger climate classification. Hydrol. Earth Syst. Sci. Discussions, 11(5), 1633-1644, 2007, hal-00305098.

WMO: Technical Note No. 172, WMO-No. 554, World Meteorological Organization, Geneva, Switzerland, 121-123, 1981.

WMO: Guide to meteorological instruments and methods of observation, WMO-No 8, 2008 edition updated in 2010, World Meteorological Organization, Geneva, Switzerland, 2012.

Annex A. Procedure for validation

The validation of a product is made by comparing high quality ground measurements acquired at a measuring station. These measurements are also called observations. There are several operations to perform *a)* to ensure that the observations are of sufficient quality so that they can be considered as a reference and *b)* to adapt the different time systems and samplings.

A.1 Controlling the quality of the observations and taking care of the time system

Time series of observation at stations have been screened for their quality according to the WMO procedure (1981) with details given in Korany et al. (2016). The automated procedure checks whether the observations exceed physically possible and extremely rare limits as well as tests of consistency between the various components of the radiation whenever possible and flags them as suspicious. Then an additional visual check is performed to further remove suspicious outliers.

Observations have been acquired in different time systems (UT: Universal Time, or TST: True Solar Time). No resampling of observations is performed in the procedure for validation. In the case of observations acquired in TST system, the procedure for collecting corresponding CRS data is as follows. Given the time stamp in TST, the times in UT for the beginning and the end of the observation are computed using the SG2 library (Blanc, Wald, 2012). In parallel, the CRS data are requested with a time step of 1 min in the UT system. The corresponding CRS irradiance is computed by summing up the 1 min data for the instants comprised between the two time limits.

A.2 Taking care of missing observations within an hour or one day

The validation may be performed at the sampling rate of the observations, e.g., every 1 min, 2 min, 10 min etc. It may be desirable to perform the validation at a time scale that is greater than the sampling rate, e.g. 1 h or 1 day. This necessitates summing up e.g. 60 observations at 1 min to yield the hourly irradiation.

Some of these observations will be flagged out by the quality check procedure. It comes out that some data is missing in a given hour and that the hourly irradiation cannot be computed with e.g. 60 observations made every 1 min within this hour but with less than 60. Hence, the sum of the valid observations is not the actual hourly irradiation; it will be equal or less.

One solution could be to reconstruct an hourly irradiation using e.g. the hourly profile of the extraterrestrial irradiation or of the irradiation in cloud-free case. This has been examined by the Task 36 “Solar Resource Knowledge Management” of the Solar Heating and Cooling Agreement of the International Energy Agency (2005-2010), which has recommended no to reconstruct hourly or daily irradiation from measurements with gaps.

The Task 36 has recommended instead constructing pseudo-hourly irradiation or irradiance by summing up the valid observations. A similar summation for the extraterrestrial irradiation is performed for exactly the same instants. This yields a pseudo-hourly extraterrestrial irradiation. The pseudo-hourly irradiation is valid only if the pseudo-hourly extraterrestrial irradiation is equal to or greater than 0.9 times the actual hourly extraterrestrial irradiation. This constraint is set to avoid extreme cases at sunrise and sunset. Invalid pseudo-hourly observations are rejected from the analysis. The same procedure applies to the daily irradiation if needed.

Pseudo-hourly irradiations from estimates are constructed in the same way.

A.3 Pairing observations and estimates

At that stage, two data sets are available. The first one contains original observations, or pseudo-hourly or pseudo-daily irradiations, depending on the case. Only valid observations have been retained. The second one is made of the original estimates, or pseudo-hourly or pseudo-daily irradiations, depending on the case. Only valid observations and estimates have been retained in these data sets.

For the sake of the simplicity, observations and estimates, respectively, will denote either the original observations and estimates, or the pseudo-hourly or pseudo-daily irradiations.

For each instant of valid observation, an observation is paired to the estimate from the product made at the location of the station and this instant. Only pairs are kept for the validation.

A.4 Overview of the procedure for validation

The procedure for validation comprises two parts. In the first one, differences between estimates and observations are computed and then summarized by classical statistical quantities. In the second part, statistical properties of estimates and observations are compared.

The procedure for validation applies to irradiation or irradiance, and clearness index. The changes in solar radiation at the top of the atmosphere due to changes in geometry, namely the daily course of the sun and seasonal effects, are usually well reproduced by models and lead to a de facto correlation between observations and estimates of irradiation. The clearness index is a stricter indicator of the performances of a model regarding its ability to estimate the optical state of the atmosphere. Though the clearness index is not completely independent of the position of the sun, the dependency is much less pronounced than for radiation.

A.5 Computation of deviations and statistical quantities

This part of the present protocol of validation puts one more constraint on observations.

Valid before 2020Q4 validation report (until DJF 2020):
Since the lowest values can be noise and are therefore insignificant in a validation process, any observation should be greater than a minimum significant value. If there are not, the observations, and the corresponding estimates, are removed from the data sets and are not kept for the computation of the deviations.

The threshold is selected in such a way such that there is a 99.7 % chance that the actual irradiance is significantly different from 0 and that it can be used for the comparison. It is set to 1.5 times the uncertainty of measurements of good quality as reported by the WMO (2012).

The threshold is 30 W m^{-2} (1.5 times 20 W m^{-2}) for the hourly (or intra-hourly) mean of global or diffuse irradiance and 7.5 W m^{-2} (1.5 times 5 W m^{-2}) for the daily mean of global or diffuse irradiance. As for the direct irradiance at normal incidence, the threshold was set to 22 W m^{-2} (1.5 times 15 W m^{-2}) for the hourly or intra-hourly mean and 7.5 W m^{-2} (1.5 times 5 W m^{-2}) for the daily mean.

December 2020 - change in the validation protocol on usage of lower thresholds:
From #30 report (MAM 2020 dataset) onwards, no threshold on irradiance value is applied to *B* anymore. A new threshold on solar elevation (>10°) is applied on all components in order to avoid horizon obstructions and directional response of pyranometers. This new protocol is based on a recent study comparing the effect of different thresholds on the validation. The results for the *B* component are presented in the report CAMS72_2018SC2_D72.1.6.1-2020, the Service update report 2020.
From this report #31 2021Q1 (JJA 2020 dataset) onwards, no threshold on irradiance value is applied to *G* and *D* anymore, in order to be consistent with *B*. The quality check procedure used to remove all *G* under 50 W m^{-2}, for the reason that under this value the tests cannot be performed. That also automatically removes *D* under 15 W m^{-2} approximately. Actually, it is unclear whether the data outside of the tested domain should be re-integrated into the dataset. A collaboration with the IEA PVPS task16 team for that (and other) unclear issues is foreseen. For the consistency of all components, the data outside the tested domain are re-integrated in the dataset.

Following the ISO standard (1995), the deviations are computed by subtracting observations for each instant from the estimates: deviation = estimate - observation. The set of deviations is summarized by a few quantities such as the bias or the root mean square error listed in next table. 2-D histograms between observations and estimates are drawn as well as histograms of the deviations.

Quantities summarizing the deviations

Mean of measurements at station kept for validation	The mean of the measurements made at the station and kept for validation for this period.
Number of data pairs kept for validation	The number of couples of coincident data (CRS, ground measurements) used for validation.
Percentage of data pairs kept relative to the number of original measurements	The number of couples of coincident data (CRS, ground measurements) kept divided by the number of measurements available and greater than 0 from the station.
Bias (positive means overestimation)	The mean error for the period, i.e. the mean of the deviations. It is also equal to the differences between the mean of the CRS product and the mean of the ground measurements. The bias denotes a systematic error. Ideal value is 0.
Bias relative to the mean of measurements	The bias divided by the mean of measurements kept for validation, expressed in per cent.
RMSE	The root mean square error. Deviations are squared then averaged, and the RMSE is the root of this average. Ideal value is 0.
RMSE relative to the mean of measurements	The RMSE divided by the mean of measurements kept for validation, expressed in per cent.
Standard deviation	The bias is subtracted from each deviation. The result is squared and averaged. The standard deviation is the root of this average. It denotes the scattering of the deviations around the bias. Ideally, the standard deviation of deviations must be close to 0, and more exactly within the standard deviation of the errors of the measurements.
Relative standard deviation	The standard deviation divided by the mean of measurements kept for validation, expressed in per cent.
Correlation coefficient	The correlation coefficient between the CRS data and the ground measurements. It denotes how well the CRS product reproduces the change in measurements with time. The closer to 1 the correlation coefficient, the better the reproduction of the variability.

Formula to compute the above-mentioned quantities

Formula	
At instant k, observation is x_k and estimate (model) is y_k	
Number of samples	N pairs of coincident values (x_k, y_k)
Mean observed value	$m_x = \frac{1}{N}\sum_{k=1}^{N} x_k$
Mean of the estimates y	$m_y = \frac{1}{N}\sum_{k=1}^{N} y_k$
Deviation at k	$\delta_k = (y_k - x_k)$
Bias (mean deviation, systematic error)	$b = \frac{1}{N}\sum_{k=1}^{N} \delta_k$
Relative bias	$rb = {}^{b}/_{m_x}$
Root mean square error	$RMSE = \sqrt{\frac{1}{N}\sum_{k=1}^{N} \delta_k^2}$
Relative RMSE	$rRMSE = {}^{RMSE}/_{m_x}$
Standard deviation of δ	$\sigma = \sqrt{\frac{1}{N}\sum_{k=1}^{N} (\delta_k - b)^2}$
Relative standard deviation	$r\sigma = {}^{\sigma}/_{m_x}$
Relation between b, $RMSE$ and σ	$RMSE^2 = b^2 + \sigma^2$
Standard deviation of x	$\sigma_x = \sqrt{\frac{1}{N}\sum_{k=1}^{N} (x_k - m_x)^2}$
Standard deviation of y	$\sigma_y = \sqrt{\frac{1}{N}\sum_{k=1}^{N} (y_k - m_y)^2}$
Covariance of x and y	$\sigma_{xy} = \frac{1}{N}\sum_{k=1}^{N} (x_k - m_x)(y_k - m_y)$
Correlation coefficient	$CC = {}^{\sigma_{xy}}/_{\sigma_x \sigma_y}$

Assuming that the observations achieve the “moderate quality” pyranometer measurements defined by WMO (2008, rev. 2012) for hourly global radiation, one may ask if the CRS estimates are compliant with “moderate quality”. Defined as the 95 % probability (P95), the relative uncertainty for “moderate quality” should not exceed 20 %. The total uncertainty takes into account the uncertainty of observations and the uncertainty of the estimates. It can be expressed in a first approximation as the quadratic sum of both uncertainties. As a consequence, the total relative uncertainty should not exceed 28 % (P95), or 14 % (P66) if the estimates were of “moderate” quality.

A.6 Typical uncertainty of measurements

The World Meteorological Organization (WMO, 2012) sets recommendations for achieving a given accuracy in measuring solar radiation. This document clearly states that “good quality measurements are difficult to achieve in practice, and for routine operations, they can be achieved only with modern equipment and redundant measurements.” The following Tables report the

typical uncertainty (95 % probability) that can be read in the WMO document. Uncertainties are expressed in J m^{-2} in the original document. The following Tables report them in W m^{-2} also.

Table A.1. Typical uncertainty (95 % probability) of measurements made by pyranometers (source: WMO 2012)

	Good quality	**Moderate quality**
Hourly irradiation	8 % if irradiation is greater than 0.8 MJ m^{-2}. Otherwise uncertainty is 0.06 MJ m^{-2}, i.e. 6 J cm^{-2}, or for irradiance approx. 20 W m^{-2}	20 % if irradiation is greater than 0.8 MJ m^{-2}. Otherwise uncertainty is 0.16 MJ m^{-2}, i.e. 16 J cm^{-2}, or for irradiance approx. 50 W m^{-2}
Daily irradiation	5 % if irradiation is greater than 8 MJ m^{-2}. Otherwise, uncertainty is set to 0.4 MJ m^{-2}, i.e. 40 J cm^{-2}, or for irradiance approx. 5 W m^{-2}	10 % if irradiation is greater than 8 MJ m^{-2}. Otherwise, uncertainty is set to 0.8 MJ m^{-2}, i.e. 80 J cm^{-2}, or for irradiance approx. 9 W m^{-2}

Table A.2. Typical uncertainty (95 % probability) of measurements made by pyrheliometers (source: WMO 2012)

	High quality	**Good quality**
1 min irradiation	0.9 % 0.56 kJ m^{-2}, or approx. 9 W m^{-2}	1.8 % 1 kJ m^{-2}, or approx. 17 W m^{-2}
Hourly irradiation	0.7 % 21 kJ m^{-2}, or approx. 6 W m^{-2}	1.5 % 54 kJ m^{-2}, or approx. 15 W m^{-2}
Daily irradiation	0.5 % 200 kJ m^{-2}, or approx. 2 W m^{-2}	1.0 % 400 kJ m^{-2}, or approx. 5 W m^{-2}

A.7 Definitions of a few quantities in solar radiation

The hourly global irradiation $G_{energy}h$ is the amount of energy received during 1 h on a horizontal plane at ground level. It is also known as hourly global horizontal irradiation, or hourly surface solar irradiation. The hourly diffuse irradiation $D_{energy}h$ is the amount of energy received from all directions of the sky vault, except that of the sun, during 1 h on a horizontal plane at ground level, and the hourly direct (or beam) irradiation $B_{energy}h$ is the amount of energy received from the direction of the sun during 1 h on this horizontal plane.

The hourly global irradiation $G_{energy}h$ is the sum of $B_{energy}h$ and $D_{energy}h$:
$G_{energy}h = B_{energy}h + D_{energy}h$

The hourly mean of global irradiance *G*h, respectively direct irradiance $B_{horizontal}$h and diffuse irradiance *D*h, is equal to G_{energy}h, respectively B_{energy}h and D_{energy}h, divided by 3600 s. If the irradiation is expressed in Wh m^{-2}, then the dividing duration is not 3600 s, but 1 h, yielding irradiance in W m^{-2}.

The hourly mean of direct irradiance at normal incidence *B*h is the irradiance received from the direction of the sun during one hour on a plane always normal to the direction of the sun. See Blanc et al. (2014) for more details on the definition of the direct irradiance at normal incidence and the incidence of the circumsolar radiation.

For the sake of simplicity, the notation *h* is abandoned in this text from now on. The hourly means of global and diffuse irradiances are noted *G* and *D*, and the hourly mean of the direct irradiance at normal incidence is noted *B*.

The hourly clearness index *KT* is defined as the ratio of *G* to the hourly extra-terrestrial irradiance *G0*: *KT* = *G* / *G0*. The extra-terrestrial irradiance is computed here by the means of the SG2 algorithm (Blanc, Wald, 2012). The direct clearness index and the diffuse clearness index are defined in a similar way. Because the ratio of the direct horizontal to the direct normal is equal to the cosine of the solar zenithal angle at both ground level and top of atmosphere, it comes that the direct clearness index is the same than the direct normal clearness index.

Annex B. Station validation reports for this quarter

The validation reports provide histograms of irradiances and clearness indices computed for both observations and CRS estimates, as well as monthly means and standard deviations of hourly means of irradiance for each month of the period.

This document only includes an example of the validation report for this quarter and for a single station (Kishinev). Similar reports for all stations listed in Table 2.1 are available in pdf format in the supplement zip archive:

CAMS72_2018SC2_D72.1.3.1-2021Q1_annexB_stationwise/
CAMS72_2018SC2_D72.1.3.1-2021Q1_annex_B_JJA2020_STATIONNAME.pdf

Annex B. Station KISHINEV

SOLAR RADIATION VALIDATION REPORT

CAMS Radiation Service (CRSv3.2) - Hourly Mean of Irradiance
KISHINEV - Moldova
Latitude: 47.001°N; Longitude: 28.816°E; Elevation a.s.l.: 205.0 m
From 2020-06 to 2020-08

This document reports on the performance of the product CAMS Radiation Service (CRSv3.2) when compared to high quality measurements of solar radiation made at the station of KISHINEV from 2020-06 to 2020-08 using a standard validation protocol.

Report generated on 2021-03-20

I. Summary of performance

Summary of the performances of the CRSv3.2 product for Hourly Mean of Irradiance at KISHINEV

	Global	Diffuse	Direct Normal	Unit
Mean of measurements at station kept for validation	491	148	513	W/m²
Number of data pairs kept for validation	1160	1160	1160	
Percentage of data pairs kept relative to the number of data >0 in the period	100	100	100	
Percentage of data pairs kept relative to the number of valid instants in the period	97	97	97	%
Bias (positive means overestimation; ideal value is 0)	-6	10	-16	W/m²
Bias relative to the mean of measurements	-1	7	-3	%
RMSE (ideal value is 0)	87	47	141	W/m²
RMSE relative to the mean of measurements	18	31	27	%
Standard deviation (ideal value is 0)	87	46	140	W/m²
Relative standard deviation	18	32	27	%
Correlation coefficient (ideal value is 1)	0.940	0.871	0.886	

II. 2-D histograms (scatter density plots) - Histogram of deviations

The 2-D histogram, also known as scatter density plot, indicates how well the estimates given by CRSv3.2 match the coincident measurements on a one-to-one basis. Colors depict the number of occurrences of a given pair (measurement, estimate). In the following, yellow is used for the least frequent pairs, with blue for intermediate frequencies and blue for the highest-frequency pairs. Ideally, the dots should lie along the red line. Dots above the red line mean an overestimation. Dots below the red line denote an underestimation. The mean of the measurements, the bias, the standard-deviation and the correlation coefficient are reported. The blue line is the affine function obtained by the first axis of inertia minimizing the bias and the standard-deviation. Ideally, this line should overlay the red line. The blue line shows the trend in error when values are far off the mean of the measurements.

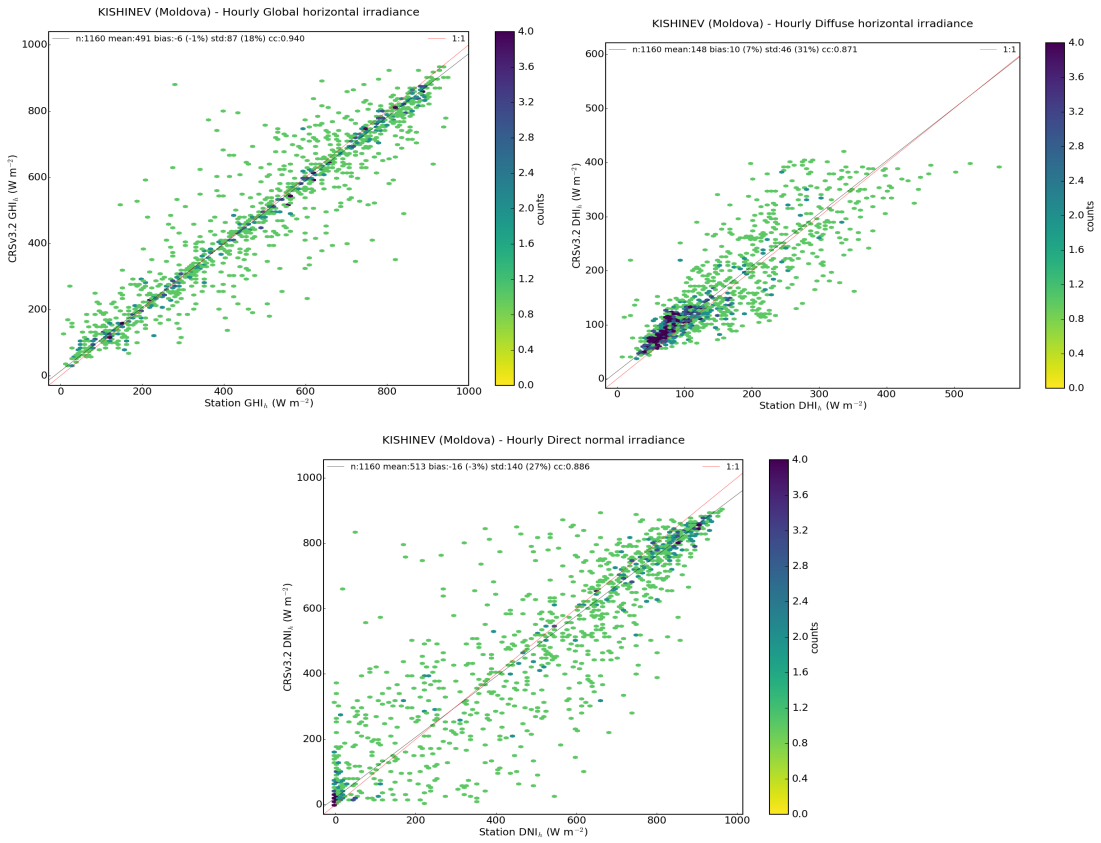

Figure 1. 2-D histogram between ground measurements (station) and the CRSv3.2 product for Hourly Mean of Irradiance

The histogram of the deviations, or as below the frequency distribution of the deviations, indicates the spreading of the deviations and their asymmetry with respect to the bias. Ideally, frequency should be 100% for deviation equal to 0. The more compact the frequency distribution of the deviations, the better.

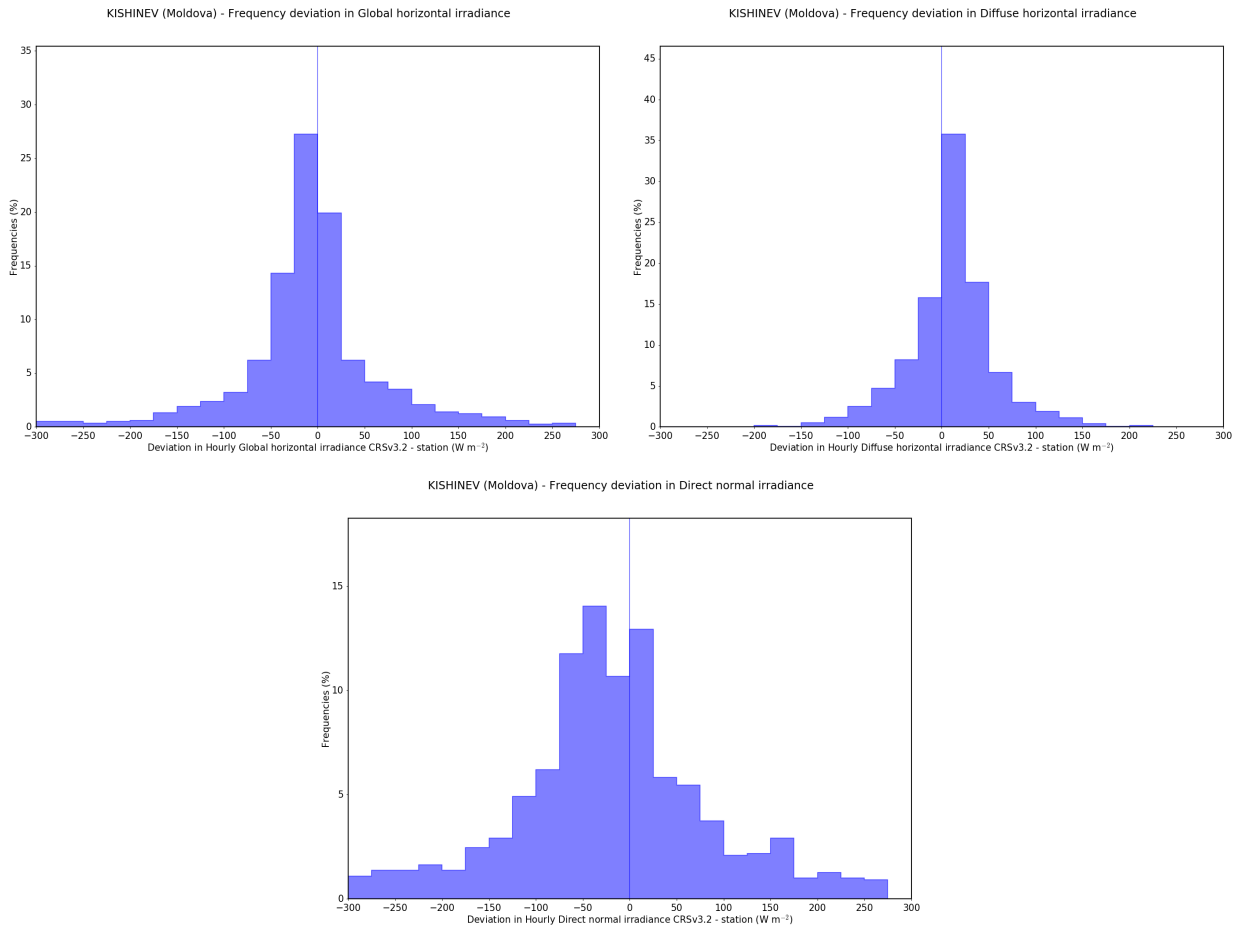

Figure 2. Frequency distribution of the deviations (CRSv3.2 - measurements)

III. Comparison of histograms

The graphs above deal with comparisons of measurements and CRSv3.2 values on a one-to-one basis: for each pair of coincident measurement and CRSv3.2 estimate, a deviation is computed and the resulting set of deviations is analysed.

This section deals with the statistical representativeness of the measurements by CRSv3.2. The frequency distributions of the measurements at station (red line) and the estimates (blue line) are computed and compared. A frequency distribution (histogram) shows how Hourly Mean of Irradiance values are distributed over the whole range of values. Ideally, the blue line should be superimposed onto the red one. If the blue line is above the red one for a given sub-range of values, it means that CRSv3.2 produces these values too frequently. Conversely, if the blue line is below the red one, CRSv3.2 does not produce values in this sub-range frequently enough.

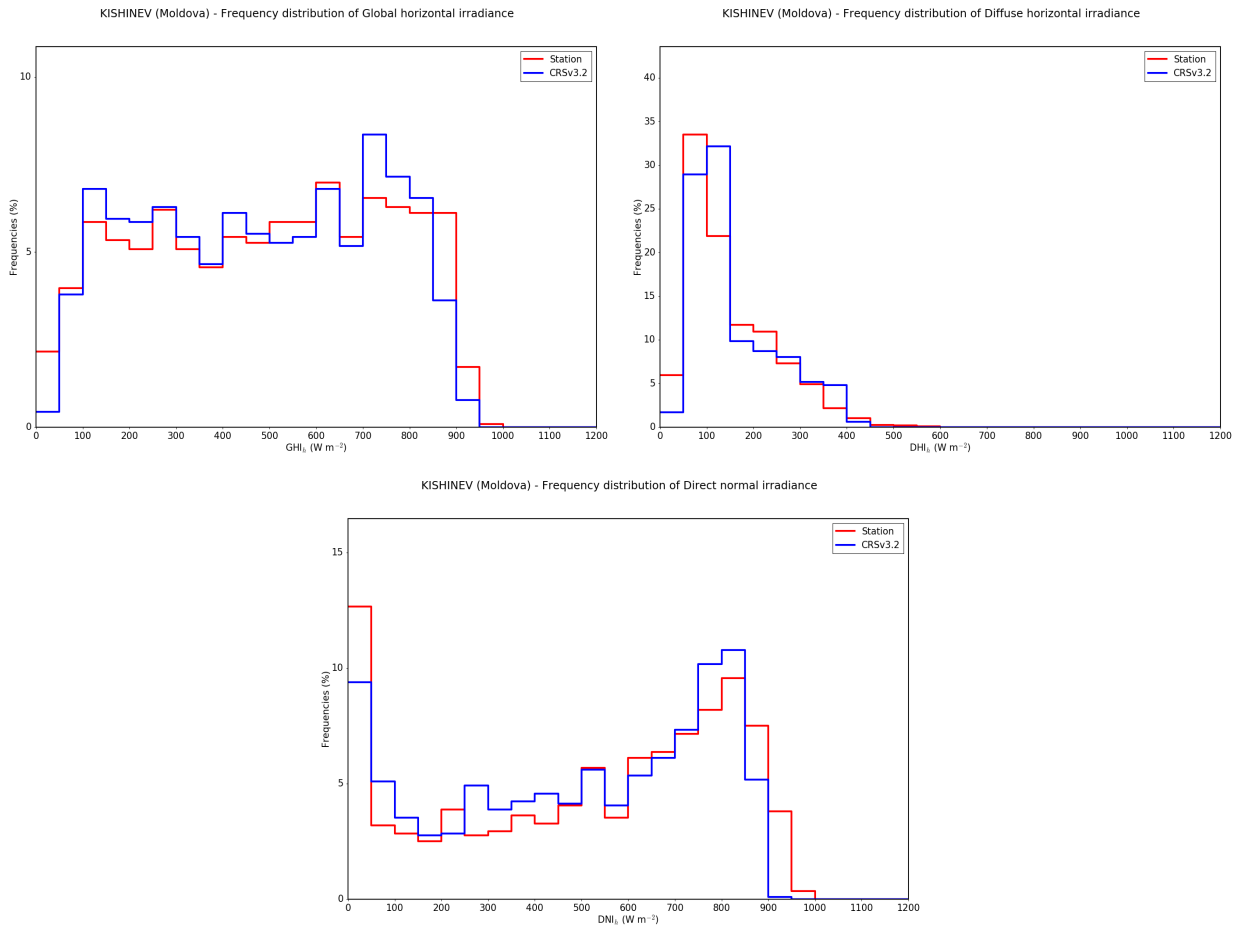

Figure 3. Frequency distributions of the measurements station (red line) and CRSv3.2 (blue line) for Hourly Mean of Irradiance

IV. Comparison of monthly means and standard deviations

For each calendar month (i.e., Jan, Feb, Mar…) in the selected period, all measurements kept for validation and the coincident CRSv3.2 estimates were averaged to yield the monthly means of Hourly Mean of Irradiance and the standard deviations. The standard-deviation is an indicator of the variability of the radiation within a month. In the following graph, monthly means are shown with diamonds and standard deviations as crosses. Red color is for measurements and blue color for CRSv3.2. The closer the blue symbols (CRSv3.2) to the red ones (measurements), the better. A difference between red dot (measurements) and blue diamond (CRSv3.2) for a given month denotes a systematic error for this month: underestimation if the blue diamond is below the red dot, overestimation otherwise. For a given month, a blue cross above the red one means that CRSv3.2 produces too much variability for this month. Conversely, CRSv3.2 does not contain enough variability in the opposite case.

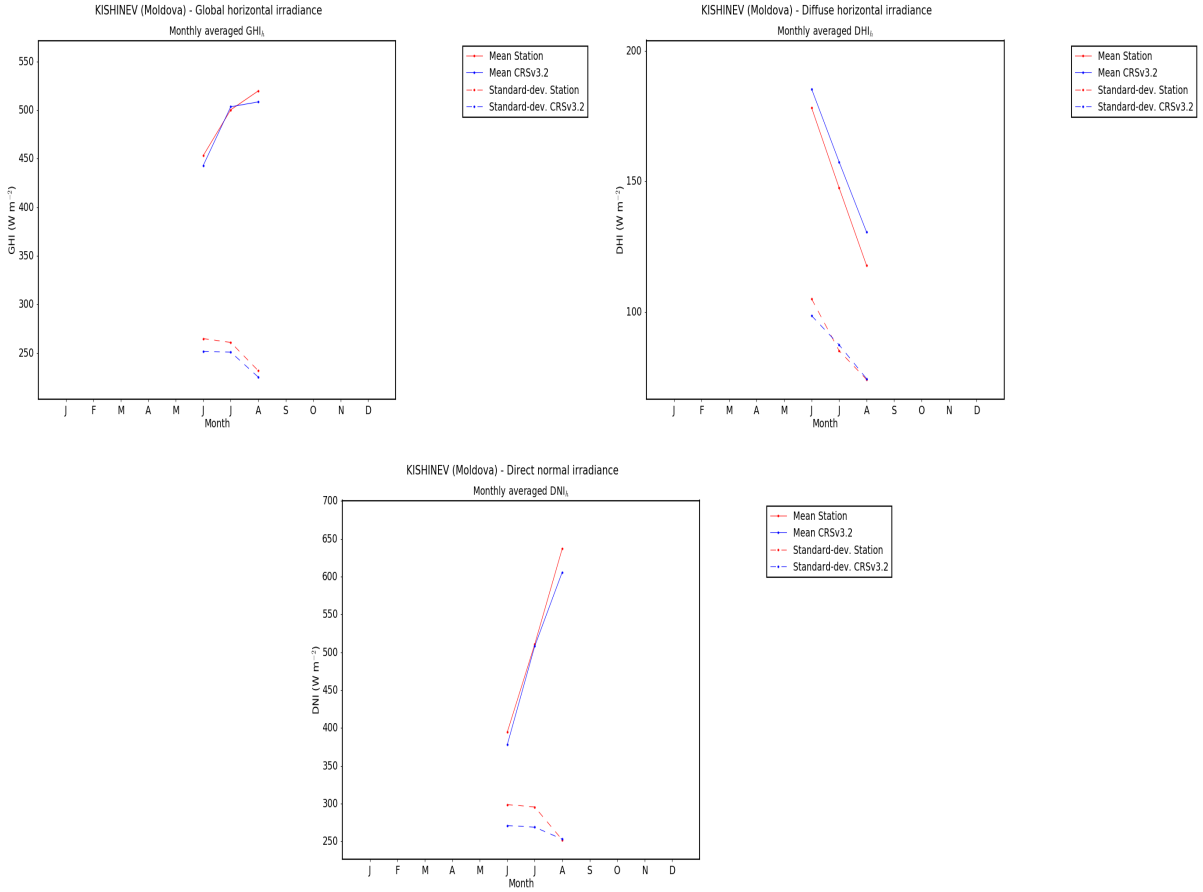

Figure 4. Monthly means of Hourly Mean of Irradiance measurements at station (red dots) and CRSv3.2 (blue diamonds), and monthly standard-deviation of measurements (red crosses) and CRSv3.2 (blue crosses)

V. Performances in clearness index

V.1. Summary of performances

Summary of the performance of the CRSv3.2 product for Hourly Mean of Clearness Index at KISHINEV

	Global	Diffuse	Direct Normal	Unit
Mean of measurements at station kept for validation	0.592	0.194	0.388	
Number of data pairs kept for validation	1160	1160	1160	

Percentage of data pairs kept relative to the number of data >0 in the period	100	100	100	
Percentage of data pairs kept relative to the number of valid instants in the period	97	97	97	%
Bias (positive means overestimation; ideal value is 0)	-0.017	0.004	-0.012	
Bias relative to the mean of measurements	-3	2	-3	%
RMSE (ideal value is 0)	0.138	0.072	0.106	
RMSE relative to the mean of measurements	23	37	27	%
Standard deviation (ideal value is 0)	0.137	0.072	0.106	
Relative standard deviation	23	37	27	%
Correlation coefficient (ideal value is 1)	0.721	0.714	0.886	

V.2. 2-D histograms (scatter density plots) - Comparison of histograms

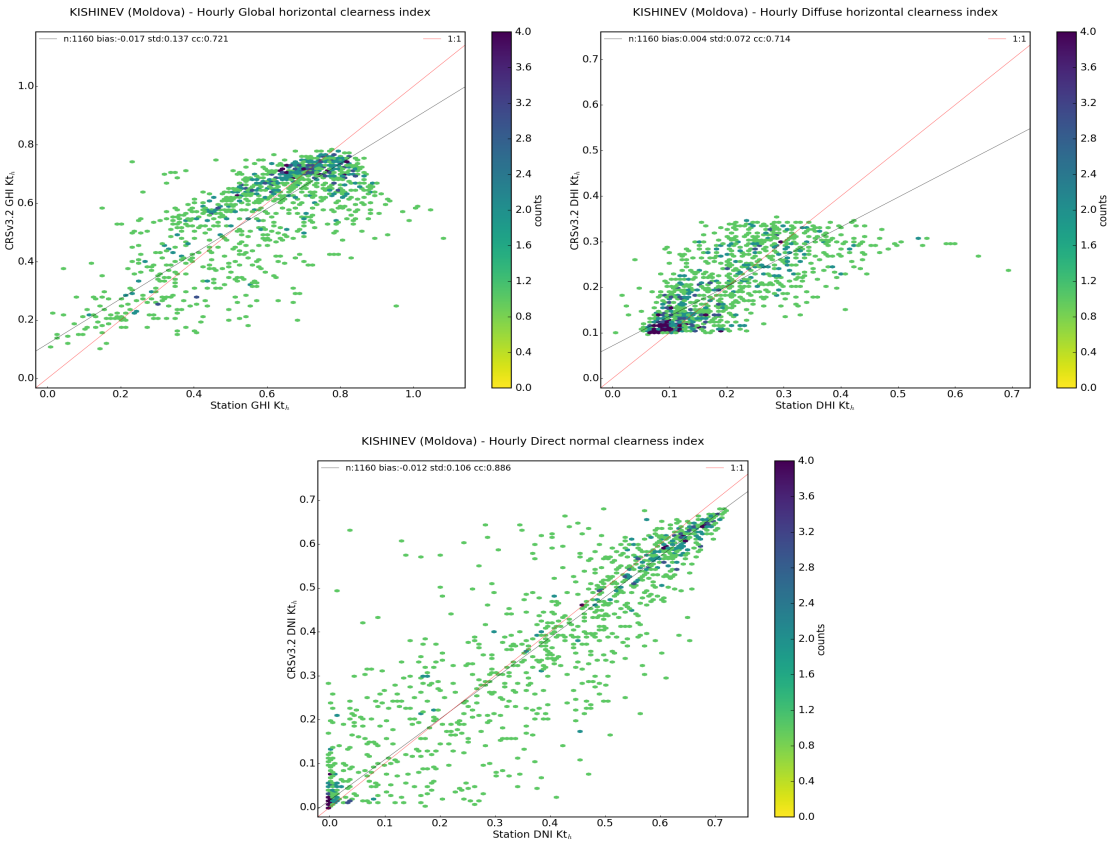

Figure 5. 2-D histogram between ground measurements (station) and the CRSv3.2 product for Hourly Mean of Clearness Index

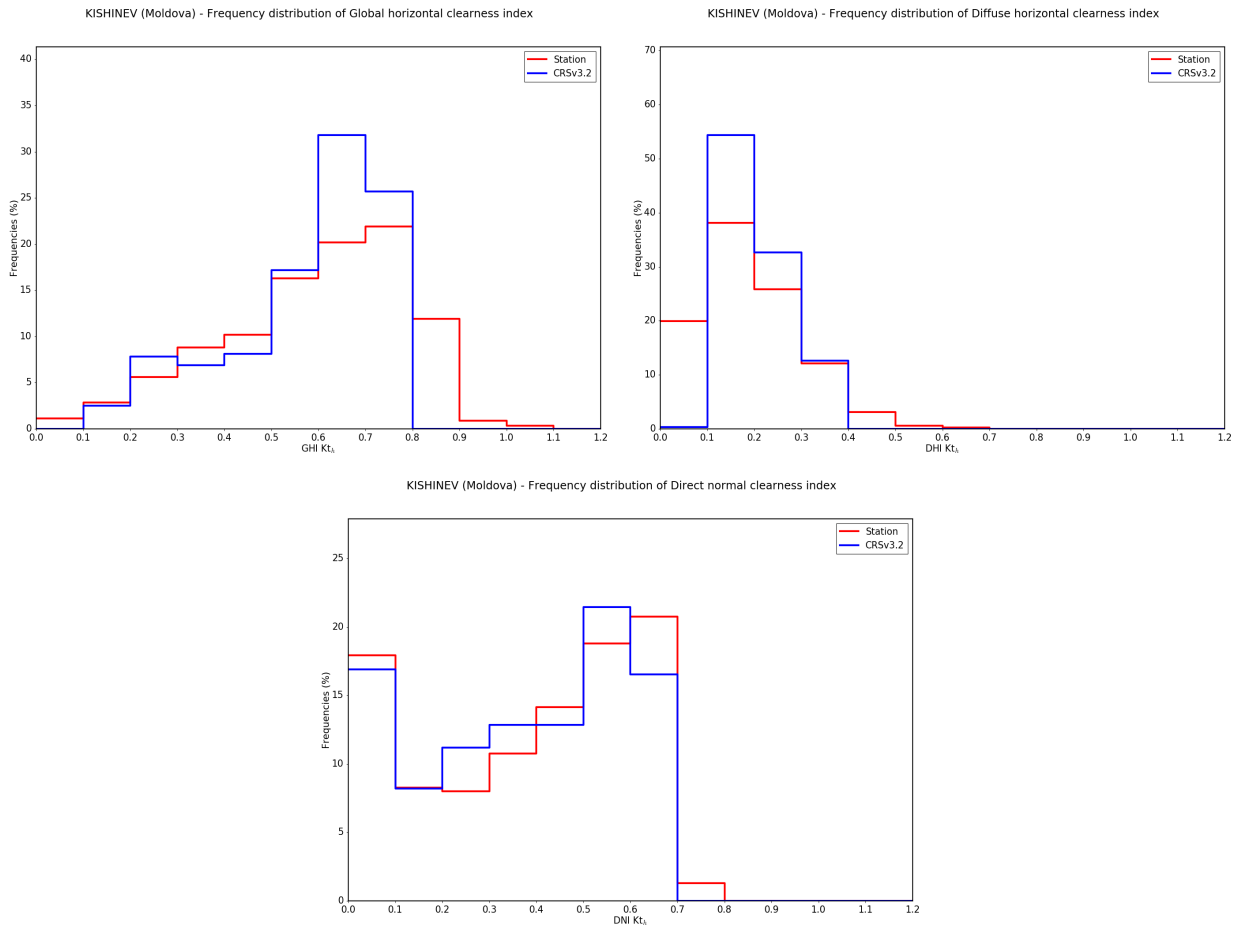

Figure 6. Frequency distributions of the measurements station (red line) and CRSv3.2 (blue line) for Hourly Mean of Clearness Index

Copernicus Atmosphere Monitoring Service

ECMWF - Shinfield Park, Reading RG2 9AX, UK

Contact: info@copernicus-atmosphere.eu

atmosphere.copernicus.eu copernicus.eu ecmwf.int